Gravity and Ground Magnetic Data from Selected Traverses in the Amargosa Desert and Vicinity, Nevada and California

By Edward A. Mankinen[1], Donald S. Sweetkind[2], Edwin H. McKee[1], and Robert L. Morin[1]

Open-File Report 2005–1444

2005

Any use of trade, firm, or product names is for descriptive purposes only and does not imply endorsement by the U.S. Government.

U.S. DEPARTMENT OF THE INTERIOR
U.S. GEOLOGICAL SURVEY

[1]USGS, 345 Middlefield Road, Menlo Park, California 94025
[2] USGS, P.O. Box 25046, Denver, Colorado 80225

TABLE OF CONTENTS

ABSTRACT …… 1

INTRODUCTION …… 1

ACKNOWLEDGMENTS …… 2

REGIONAL FRAMEWORK …… 2

PROCEDURES …..…….. 3

GRAVITY DATA …….. 4

MAGNETIC DATA …….. 5

GROUND MAGNETIC PROFILES …….. 6

TRAVERSES IN THE VICINITY OF HIGHWAY 95 ……. 6

TRAVERSES IN THE NORTHWEST PART OF THE AMARGOSA DESERT …….. 7

TRAVERSES ALONG THE NORTHEAST EDGE OF THE FUNERAL MOUNTAINS ……. 7

RESULTS …….…… 8

CONCLUSIONS …… 10

REFERENCES …… 11

ILLUSTRATIONS

Figure 1. Index map of SE California/SW Nevada …… 16

2. Map showing location of Amargosa Desert basin ……... 17

3. Magnetic anomalies of the study area ……...…… 18

4. Isostatic residual gravity anomalies of the study area …… 19

5. Residual magnetic anomalies of the study area …… 20

6. Portion of residual magnetic anomaly map showing detailed study areas ..……. 21

7. Residual magnetic anomaly map of Highway 95 area …….. 22

8. Gravity and magnetic profiles along “LWells” traverse …….. 23

9. Gravity and magnetic profiles along “BigDune1” traverse …… 24

10. Gravity and magnetic profiles along “BigDune2” traverse …… 25

11. Residual magnetic anomaly map of the Ashton area ……..… 26

12. Gravity and magnetic profiles along “Ashton1” traverse ...……..... 27

13. Gravity and magnetic profiles along “Ashton2” traverse ……..... 28

14. Gravity and magnetic profiles along “Ashton3” traverse ..…… 29

15. Residual magnetic anomaly map of the Funeral Mountains area ..…… 30

16. Gravity and magnetic profiles along “Leeland” traverse …….. 31

17. Gravity and magnetic profiles along “Scranton” traverse …… 32

18. Gravity and magnetic profiles along “FWell” traverse …… 33

19. Residual magnetic anomaly map of the Death Valley Junction area …..……..... 34

20. Gravity and magnetic profiles along “Ash” traverse …… 35

21. Residual magnetic anomaly map of the Ashton to Lathrop Wells area ..……..... 36

22. Geophysical forward model along geologic cross-section H6 …..……..…..... 37

TABLE

Table 1. Principal facts of gravity stations from Amargosa Desert Basin …….. 38

Gravity and Ground Magnetic Data from Selected Traverses in the Amargosa Desert and Vicinity, Nevada and California

Edward A. Mankinen, Donald S. Sweetkind, Edwin H. McKee, and Robert L. Morin

ABSTRACT

High-resolution aeromagnetic surveys of the Amargosa Desert region have revealed many magnetic anomalies of varying character. High-amplitude anomalies in the northern part of the region are produced by the volcanic rocks of the southern Nevada volcanic field (SNVF). Contrasted with these are low-amplitude anomalies over a broad area in the southern and southwestern part of the aeromagnetic survey that reflect pre-Cenozoic, largely nonmagnetic basement rocks exposed in the different ranges. More subtle, isolated anomalies are distributed throughout the region and indicate sources that are overlain by, or included within, the alluvial deposits. We have investigated some of the latter low-amplitude anomalies using gravity and magnetic techniques in an attempt to help characterize their causative bodies. Our depth-to-magnetic-source calculations indicate that the anomalies investigated have sources within the alluvial fill and agree well with results from similar studies in the region. Possible source rocks include Miocene tuff of the SNVF and/or Tertiary rocks of the Death Valley volcanic field.

INTRODUCTION

This study was undertaken as part of a project to characterize complex regional hydrogeologic environments in the southwestern United States. The Cenozoic basin that lies beneath the Amargosa Desert , herein called the Amargosa Desert basin, (figures 1 and 2) is one example of the many Cenozoic basins of the arid southwestern United States that contain significant volumes of volcanic rock within the basin fill. These volcanic rocks include thick sections of welded or non-welded tuffs, thin basaltic lava flows interlayered with sedimentary deposits, and accumulations of tephra at local volcanic centers.

Volcanic rocks can have hydrogeologic properties significantly different from the sedimentary basin fill and thus are additional important elements to be included in the hydrogeologic framework of any given basin. These concealed volcanic rocks need to be defined in terms of their location, geometry, and physical properties, even in basins with little detailed direct subsurface information. Potential field data and interpretations and models derived from those data can be an important source of information in defining the hydrology of the basin.

This report describes potential field data collection across selected magnetic anomalies and inferred faults for the purpose of better defining basin geometry and the nature of the buried volcanic rocks that are the potential sources of the magnetic anomalies. Detailed magnetic data across magnetic anomalies in the Amargosa Desert have previously been collected and analyzed by Langenheim (1995), O'Leary and others (2002), and Blakely and others (2005).

ACKNOWLEDGEMENTS

We appreciate thoughtful reviews of the manuscript by D. O'Leary and C. Roberts.

REGIONAL FRAMEWORK

The area shown in figures 1 and 2 contains several Cenozoic basins that occupy a structurally complex region in the Walker Lane belt (Stewart, 1988) along the western edge of the Basin and Range physiographic province. Neogene deformation in the region is characterized by a variety of structural patterns that overlap in space and time, including: (1) Basin and Range extension along high-angle and low-angle normal faults; (2) development of discrete strike-slip faults and transtensional basins within the Walker Lane belt (Stewart, 1988; Stewart and Crowell, 1992); and (3) volcanism that preceded and temporally overlapped regional extension and emanated from volcanoes that collapsed to form caldera complexes of the southwestern Nevada volcanic field (Sawyer and others, 1994) to the north of the Amargosa Desert, and from smaller volcanic centers within the central Death Valley volcanic field (Wright and others, 1991) to the south of the Amargosa Desert. The SNVF was most active between ~15 and ~7 Ma. The waning stages of volcanism during Plio-Pleistocene time have produced basalt lava flows, dikes, and basaltic cinder cones in the Yucca Mountain–Crater Flat area. These post-caldera basalts range in age from Late Miocene to Quaternary (Crowe and others, 1995) and form local flows and cinder cones.

Cenozoic basins within this region display a wide range of tectonic styles from normal-faulted basins with half-graben geometry, to complex transtensional basins associated with strike slip faults. The Amargosa Desert basin is most like a rift or full graben and thus somewhat different from the other transtensional pull-apart basins to the west. This feature has been variously referred to as the Amargosa Desert rift (Wright, 1989), the Kawich-Greenwater rift (Carr, 1990), and the central Amargosa trough (Fridrich, 1999). Rocks in the ranges surrounding the Cenozoic basins are varied and have a wide range of magnetizations and densities. Most of the mountain ranges that bound the Amargosa Desert expose Late Proterozoic to Cambrian quartzose and carbonate rocks (fig. 1). The quartzose rocks in places contain thin, weakly magnetic interbeds of dolomite (Hillhouse and Morin, 2003) but generally these rocks are magnetically quiet. The Amargosa Desert basin is bordered by the Miocene and Pliocene volcanic rocks of the southwestern Nevada volcanic field (Sawyer and others, 1994) on the north and the central Death Valley volcanic field (Wright and others, 1991) on the south; these volcanic rocks create pronounced high-amplitude, short wavelength magnetic anomalies (Blakely and others, 2000) (fig. 3). The general absence of strong magnetic anomalies in the vicinity of the Amargosa Desert implies that strongly magnetic volcanic rocks from either field are thin or absent (Blakely and others, 2000). Boreholes drilled within the two volcanic fields penetrate volcanic rocks or interbedded sedimentary and volcanic rocks, whereas boreholes drilled in the center of the Amargosa Desert basin typically intercept only sedimentary rocks. Volcanic rocks are present in the subsurface in the northwestern arm of the Amargosa Desert basin based on aeromagnetic data (fig. 3), borehole intercepts and on isolated outcrops of Miocene Timber Mountain Group tuffs. Locally present within the basin fill are basaltic volcanic centers, as indicated by the presence of small circular magnetic anomalies (Langenheim, 1995; O'Leary and others, 2002) or by outcrops of basalt.

PROCEDURES

Gravity data were obtained using a LaCoste and Romberg meter (USGS meter G8) and observed gravity values were referenced to the International Gravity Standardization Net 1971 (ISGN 71) gravity datum (Morelli, 1974). Gravity observations were tied to two ISGN 71 base stations (Harris and others, 1989); the original Beatty post office (***BPO***), now the Death Valley visitor station, and ***DUNE***, west of the junction of U.S. Highway 95 and Nevada State Highway 29 in Amargosa Valley. The observed gravity value given for ***BPO*** in Harris and others (1989) has been revised to 979,566.45 mGal (D.A. Ponce, USGS, written communication, 1997).

Locations of gravity stations were determined using differential GPS, with surveyed benchmarks used for control and are accurate to within about 0.1 m, both horizontally and vertically.

Magnetic data were obtained using a portable cesium vapor magnetometer integrated with a differential GPS receiver. Because of the expected short duration of each traverse, we did not employ a stationary base-station magnetometer to record diurnal variations. Measurements were made at 1-second intervals, operating the instrument in continuous mode, along selected traverses while walking at a normal pace. Horizontal positional accuracy of the GPS readings is accurate to within about 1 m. Testing the unit over the Mount Hamilton, California gravity calibration loop (Barnes and others, 1969) indicates that elevations are accurate to about 5 m (J.E. Tilden, USGS, written communication, 2004). When tied to a known elevation, however, the accuracy improves to about 0.5 m.

Depth-to-magnetic-source calculations were made using a graphical method (Peters, 1949; Blakely, 1995). Peters' method uses a proportionality constant of 1.2 for very thin bodies and 2.0 for very thick bodies. O'Leary and others (2002) used a value of 1.2, which was appropriate when assuming that the small, isolated circular anomalies in the Amargosa Desert were due to highly magnetic, low-volume eruptions similar to those produced by the basaltic cinder cones and associated flows in Crater Flat and at Lathrop Wells. Here, however, we use a more typical of value of 1.6 (e.g., Blakely and others, 2005).

GRAVITY DATA

Observed gravity at each station was adjusted by assuming a time-dependent linear drift between readings of a base station at the start and finish of each daily survey. This adjustment compensates for drift in the instrument's spring. All gravity data and their associated parameters are given in Table 1. Observed gravity values are considered accurate to about 0.05 mGal based on repeat measurements over several mountain calibration loops (Barnes and others, 1969; Ponce and Oliver, 1981). Gravity data were reduced using standard gravity corrections (Harris and others, 1989) and a reduction density of 2670 kg/m^3. Inner-zone terrain corrections (zones A, B, C, and D of Hayford and Bowie, 1912), which are necessary to account for variations in topography near a gravity station, were obtained using a program developed by Spielman and Ponce (1984). The calculations use digitized topography in a digital elevation model (DEM) and a procedure by Plouff (1977). A regional isostatic field was calculated using an Airy-Heiskanen (Heiskanen and Vening Meinesz, 1958) model for local compensation of topographic loads (Simpson and others, 1983, 1986). This model assumes a crustal thickness of 25 km, a crustal

density of 2670 kg/m^3, and a 400 kg/m^3 density contrast between the crust and mantle. This regional isostatic field was subtracted from the complete Bouguer anomaly, thus removing long-wavelength variations in the gravity field that are inversely related to topography. The resulting isostatic residual gravity anomaly, therefore, is a reflection of local density distributions within middle to upper crustal levels. The isostatic residual gravity anomaly for the Amargosa Valley study area, incorporating the 152 new gravity observations from Table 1, is shown in figure 4. The new gravity stations were established along the same traverses as the ground magnetic profiles described in the following section and were intended to complement those data.

MAGNETIC DATA

A high-resolution aeromagnetic survey of the Amargosa Desert was flown in 1999 (Blakely and others, 2000) to aid in understanding the subsurface lithology and structure of the region. The portion of this high-resolution survey that covers our study area is shown in figure 3. Many prominent features are clearly seen on this map, such as the high-amplitude anomalies in the northern part of the study area that are produced by the volcanic rocks of the southern Nevada volcanic field (Byers and others, 1976a; 1976b; Christiansen and others, 1977; Sawyer and others, 1994). A recent high-resolution, helicopter-based magnetic survey over the northern part of the Amargosa Desert (Perry and others, 2005) confirms the location of these high-amplitude anomalies. Low-amplitude anomalies over a broad area in the southwestern part of the aeromagnetic survey probably reflect pre-Cenozoic, largely nonmagnetic basement rocks such as those beneath the Greenwater Range and vicinity. High-amplitude, short-wavelength anomalies reflecting surface and near-surface Cenozoic volcanic rocks of the central Death Valley volcanic field (Wright and others, 1991), however, punctuate the broad low-amplitude signal in this area.

Between these broad areas are many smaller, more isolated anomalies, sources of which are overlain by or included within the alluvial deposits. Some of the more subtle anomalies are more clearly delineated by analytically continuing the observed anomalies (figure 3) 100 m higher (Hildenbrand, 1983) and subtracting the result from the original grid. By removing the contribution of deeper sources (accentuated by the upward continuation) the procedure emphasizes surface and near-surface magnetic sources. The resulting magnetic residual map, extracted from Blakely and others (2000), is shown in figure 5.

The presence of small, sub-circular, generally isolated and often dipolar anomalies indicating magnetic bodies beneath the surface alluvial deposits are similar in size and shape to those associated with nearby Plio-Pleistocene subaerial basaltic volcanoes/cinder cones, and

therefore suggestive of similar sources. A number of these anomalies are shown in figure 6, labeled as in O'Leary and others (2002). O'Leary and others (2002) assigned tentative rankings to the anomalies reflecting their confidence that a given anomaly reflected a basaltic source. Their ranking scheme was: 1=high confidence, 2=probable, 3=equivocal, and 4=low confidence. Geophysical modeling (Langenheim and others, 1993; Langenheim, 1995; O'Leary and others, 2002) indicated a high degree of probability that anomalies A, B, C, D, F, G, and H reflected buried basaltic volcanic centers. Drilling into anomaly B confirmed that its source is basalt (as modeled by Langenheim and others, 1993), with an age of approximately 4.0 Ma (Carr and others, 1995). Anomaly D was ranked highest among the remaining anomalies in this group because of basalt fragments encountered in nearby drilling (Walker and Eakin, 1963).

O'Leary and others (2002) indicated a lower degree of confidence that other anomalies, some of which were modeled, reflected basaltic centers/vents. Some anomalies could be reflecting basement features and others may prove to be produced by shallow occurrences of Miocene tuff within the alluvial fill. We hoped to address some of these possibilities with some of the ground magnetic profiles described below. Other profiles cross major magnetic lineaments (Blakely and others, 2000) that possibly reflect shallow faults or fault zones. Blakely and others (2005) describe results from several ground magnetic profiles in the area, also designed to investigate some of the low-amplitude anomalies that are evident in the aeromagnetic survey.

Ground Magnetic Profiles

Nine magnetic traverses were collected in the Amargosa Desert to investigate various magnetic anomalies present within the basin. These traverses are described below.

Traverses in the vicinity of Highway 95

An east-west fault has been inferred at the north edge of the Amargosa Desert (Fridrich, 1999; Potter and others, 2002), south of Crater Flat, on the basis of the abrupt break in topography in this vicinity (figure 2), the abrupt termination of the highly magnetic, NE-trending anomalies associated with the Miocene volcanic rocks (figures 3 and 6), and the fact that the tuffs exposed at the topographic break do not represent their distal facies (Potter and others, 2002). Our traverses (labeled red lines) shown in figure 7 were designed to cross the fault informally named the Highway 95 fault by Potter and others (2002). Profiles LWells, BDune1, and BDune2 are shown in figures 8, 9, and 10, respectively. Drill holes NC-EWDP-28P (634 m total depth), NC-EWDP-15P (185 m total depth), NC-EWDP-3D (768 m total depth); 28P and 15P bottomed in Miocene

tuffs or interbedded sedimentary rocks, 3D bottomed in Cenozoic sedimentary rocks presumed to be older than volcanic rocks of the SNVF.

Traverses in the northwest part of the Amargosa Desert

Four aligned anomalies (L, M, N, O, see figure 6) were modeled as basaltic centers by O'Leary and others (2002). Using this geologic interpretation, the data were best modeled by assuming that the anomaly sources were underlain by a broader expanse of normally-magnetized Miocene welded tuff. Although their modeling was consistent with basalt sources for the anomalies, a somewhat lower degree of confidence (level 3) was expressed for this interpretation because of the irregular shapes of the anomalies and the fact that they lack definitive dipole signatures. Traverses in the Ashton area (figure 11) crossed anomaly L and boundaries of one of the broader anomalies. These traverses were also located to cross several inferred splays of the Amargosa River fault (Workman and others, 2002). Profiles Ashton1, Ashton2, and Ashton3 are shown in figures 12, 13, and 14, respectively. Drill hole BorNA-6 had a total depth of 283 m and bottomed in basin fill. Miocene welded tuffs were encountered at depths of 113 m and 213 m (Sweetkind and others, 2001a).

Traverses along the northeast edge of the Funeral Mountains

Three magnetic traverses were made on the east side of the Funeral Mountains (figure 15) and were designed to cross some of the subdued anomalies and magnetic lineaments that seem to be associated with, and truncated by, an inferred fault named the State Line fault by Blakely and others (2000). Profile Leeland (figure 16) crosses over the southern part of anomaly K of O'Leary and others (2002) and is tied to borehole BorNT-1. BorNT-1 bottomed in basin fill at 531 m. Several relatively thin tuffs, both welded and non-welded, were encountered in this borehole (Sweetkind and others, 2001a) and most likely emanated from the SNVF to the north. Note the very prominent anomalies C and D in the northeast corner of figure 15. The source for anomaly C has a reversed magnetic polarity, D a normal polarity, and both display a pronounced dipole signature. In large part because of the dipole signature, O'Leary and others (2002) expressed a high degree of confidence (level 1) that these anomalies reflected a basaltic source. Further evidence in favor of that interpretation for anomaly D was that basalt fragments were encountered in nearby drilling (Walker and Eakin, 1963). O'Leary and others had less confidence in the source for anomaly K (level 3) and noted that it also appeared to be more deeply buried than the other anomalies that they investigated.

Profile Scranton (figure 17) begins on the same anomaly that is crossed by profile FWell (figure 17) approximately 4 km to the southeast (see figure 15). This relatively long NNW-trending high is on-strike with outcrops of the Tertiary section exposed just south of the map area at Bat Mountain (Cemen and others, 1999). Although the Scranton profile crosses borehole BorNA-10, the borehole is on a smaller magnetic high to the east of the main NNW-trending anomaly. Borehole BorNA-10 encountered a single 3-m-thick welded tuff at 73 m below land surface (Sweetkind and others, 2001a) and reached a total depth of 604 m (lithology at the bottom not described in the drilling report). Profile FWell begins on a narrow north-trending positive anomaly (figure 15) and later completely crosses the prominent NNW-trending high.

In the southern-most area studied (figure 19), our gravity traverse begins approximately 2.5 km northeast of Death Valley Junction and continues into the Ash Meadows National Wildlife Refuge. Ground-magnetic profile Ash (figure 20) was located near Ash Meadows and was intended to cross magnetic anomalies associated with the State Line fault (Blakely and others, 2000). Blakely and others (2005) conducted a ground-magnetic profile (their profile DVJ) that crosses the strong north-trending anomaly near the west end of our gravity profile.

RESULTS

Our profiles in the Ashton to Lathrop Wells area (figure 21) are near geologic cross-section H6 of Sweetkind and others (2001b). Guided by their cross-section and using a commercially available 2 1/2-dimensional modeling program ("GM-SYS") based on Webring (1985), we constructed a model based primarily on forward calculations where body shapes are determined by obtaining reasonable fits between observed and calculated profiles via trial-and-error iterations. We used physical properties (density and magnetization) for the units in the area that are consistent with the modeling of O'Leary and others (2002) and Mankinen and others (2003). Aeromagnetic data along profile H6, shown in figure 22, were extracted from the aeromagnetic survey of Blakely and others (2000) and gravity observations are from the equivalent stations shown in figure 3. Result of this modeling (figure 22) is generally consistent with cross-section H6. We emphasize, however, that this solution is not unique because an infinite number of geometric models will have an associated magnetic or gravity field that closely matches the measured field. Modeling indicates two areas with reversed-polarity ash-flow tuffs (Rainier Mesa and Tiva Canyon Tuffs), beneath the area where the profile crosses Highway 95 and below the Lathrop Wells cone (also see models of O'Leary and others 2002). The sharp breaks indicated by the ground magnetic data in figures 9 and 10 may mark the southern extent of

the thickest parts of these two tuffs. The two vertical slopes along the BDune1 profile (figure 9) indicate near-surface sources. The BDune2 profile (figure 10) apparently did not extend far enough to the NE to intersect either of the features producing the BDune1 anomalies. Peters' (1949) method indicates the source for the southwestern-most anomaly at the LWells profile (figure 8) to be at a depth of ~125 m. The two other positive anomalies on the broader magnetization low along this profile indicate sources between ~250–300 m.

The ground-magnetic profile Ashton1 (figure 11) crosses a strong positive anomaly that trends north-south. The profile shows one very prominent peak with a steep western gradient (figure 12) as well as a lower-amplitude peak to its northeast. There is then a gradual decrease in intensity toward the magnetic low seen in figure 11 just SW of Highway 95. The source of the prominent anomaly at its western margin is estimated to be ~60 m below the surface, whereas the eastern margin of the lower-amplitude anomaly seems to be about 20 m deeper. Profile Ashton2 (figure 11) is roughly perpendicular to profile Ashton1 and passes southwest of the most prominent part of the N-S anomaly. The profile (figure 13) shows that the anomaly here is much broader and lower in amplitude, with its western margin ~100 m below the surface. Profile Ashton2 crosses anomaly L at its SE end. Anomaly L is estimated to be ~170 m below the surface using the ground-magnetic data, in good agreement with O'Leary and others (2002) who estimated its depth to be ~150 m based on the aeromagnetic data along a nearly perpendicular profile. Profile Ashton3 (figure 14) shows little magnetic variation until reaching a weak positive anomaly beneath drill-hole BorNA-6 (figure 11). The abrupt break at the NE end of this profile is indicative of a relatively shallow source for the anomaly although the full extent of this slope was not seen, precluding an estimate of depth-to-source. Drill hole BorNA-6 did, however, encounter the first of two welded tuffs at a depth of 113 m indicating that one (or both) of these units is probably the source of the anomaly. Both tuffs are ~30-m thick (Sweetkind and others, 2001a) indicating either that they are weakly magnetized or are of opposite polarity (i.e., the Ammonia Tanks Tuff overlying the Rainier Mesa Tuff).

Profile Leeland (figure 15) crosses the southern part of anomaly K. The ground-magnetic data are very noisy in part (figure 16), perhaps indicating that the source has been disrupted on its southern flank. The Scranton profile (figure 15) shows only a weak magnetic high (figure 17) where it crosses the small anomaly upon which borehole BorNA-10 is located. The source of the high is roughly 150 m deep, suggestive that the 3-m-thick welded tuff encountered at ~75 m down hole (Sweetkind and others, 2001a) may not be the source of this anomaly. The steeper gradient near the NE end of the profile (figure 15) may reflect the State Line fault–the source of this anomaly is estimated to be ~60 m below the surface. Profile FWell crosses a prominent

NNW-trending high (figure 15) that, like the Ashton1 profile above, appears to be a single anomaly on the aeromagnetic survey but a more complicated structure is seen with the ground-magnetic survey (figure 18). The western slope of the SW-most anomaly indicates a depth-to-source of ~50 m, the eastern slope of the anomaly to the NE indicates a source at ~100 m. The possible sources for these anomalies are unknown–the Tertiary section at Bat Mountain contains only a thin tuff (~25 Ma old) and two boreholes (Sweetkind and others, 2001a) about 5 km away from the anomalies and to the east of Bat Mountain did not penetrate any rhyolitic tuff or basalt flow in the upper 500 m of section.

Profile Ash northeast of Death Valley Junction (figure 19) shows no pronounced anomaly in the ground-magnetic data (figure 20). Note that the gradual rise in the magnetic signal essentially mimics the rise in observed gravity. Both quantities seem to be reflecting a rise in pre-Cenozoic basement based on a recent inversion of gravity data (V. Langenheim, USGS, written communication, 2004) using the method of Jachens and Moring (1990). According to this inversion, basement increases from about 1.2 km at the start of the profile, to as little as 400 m near the bend in section before gradually decreasing again to between 550 and 600 m. Our ground-magnetic data are similar to those seen in the Devils Hole profile of Blakely and others (2005) just north of our Ash profile (figure 19). Blakely and others (2005) conclude, from the absence of significant anomalies in the data along their profile, that the aeromagnetic anomalies are not reflecting variations in lithology of pre-Tertiary rocks in this area.

CONCLUSIONS

We have investigated several low-amplitude aeromagnetic anomalies in the Amargosa Desert–Ash Meadows area by establishing new gravity stations and ground-magnetic measurements along selected traverses. Although the anomalies are clearly delineated by the magnetic data, none exhibit corresponding variations in the gravity measurements. This indicates that the causative sources have densities that are comparable with the average density of the surrounding rocks. Our depth-to-magnetic-source calculations using Peters' (1949) method range from as little as 50 m to approximately 300 m. These estimates should be considered as approximations only (e.g., Blakely, 1995), however, all of the estimates indicate that the causative sources must lie at generally high stratigraphic levels within the alluvial fill. A similar conclusion was reached by O'Leary and others (2002) who investigated the high-amplitude anomalies near Yucca Mountain, and by Blakely and others (2005) based on their ground-magnetic traverses of low-amplitude anomalies in the Death Valley–Ash Meadows area.

Modeling of isolated, high-amplitude anomalies indicate strongly-magnetic sources such as buried basalt (O'Leary and others, 2002) whereas the low-amplitude anomalies are most likely caused by relatively weaker sources such as Miocene siliceous tuff of the SNVF and/or the Tertiary rocks of the Death Valley volcanic field. Densities of ash-flow tuff units in this part of Nevada have been found to be low enough, in places, to be comparable with the average density of basin sediment-fill and thus not detectable by the gravity method.

REFERENCES

Barnes, D.F., Oliver, H.W., and Robbins, S.L., 1969, Standardization of gravimeter calibrations in the Geological Survey: Eos, Transactions of the American Geophysical Union, v. 50, p. 526-527.

Blakely, R.J., 1995, *Potential Theory in Gravity and Magnetic Applications*: Cambridge University Press, 441 p.

Blakely, R.J., Hillhouse, J.W., and Morin, R.L., 2005, Ground-magnetic studies of the Amargosa Desert region, California and Nevada: U.S. Geological Survey Open-File Report 2005-1132, 23 p.

Blakely, R.J., Langenheim, V.E., Ponce, D.A., and Dixon, G.L., 2000, Aeromagnetic survey of the Amargosa Desert, Nevada and California: A tool for understanding near-surface geology and hydrology: U.S. Geological Survey Open-File Report 00-188, 35 p.

Byers, F.M., Jr., Carr, W.J., Orkild, P.P., Quinlivan, W.D., and Sargent, K.A., 1976a, Volcanic suites and related cauldrons of Timber Mountain–Oasis Valley caldera complex, southern Nevada: U.S. Geological Survey Professional Paper 919, 70 p.

Byers, F.M., Jr., Carr, W.J., Christiansen, R.L., Lipman, P.W., Orkild, P.P., and Quinlivan, W.D., 1976b, Geologic map of the Timber Mountain caldera area, Nye County, Nevada: U.S. Geological Survey Miscellaneous Investigations Map I-891, scale 1:48,000.

Carr, W.J., 1990, Styles of extension in the Nevada Test Site region, southern Walker Lane Belt—An integration of volcano-tectonic and detachment fault models, *in* Wernicke, B.P., ed., Basin and Range extensional tectonics near the latitude of Las Vegas, Nevada: Geological Society of America Memoir 176, p. 283–303.

Carr, W. J., Grow, J. A. and Keller, S. M., 1995, Lithologic and geophysical logs of drill holes Felderhoff Federal 5-1 and 25-1, Amargosa Desert, Nye County, Nevada: U.S. Geological Survey Open-File Report 95-155, 14 p.

Cemen, I., Wright, L.A., and Prave, A.R., 1999, stratigraphy, and tectonic implications of the latest Oligocene and early Miocene sedimentary succession, southernmost Funeral Mountains, Death Valley region, California, *in* Wright, L.A., and Troxel, B.W., eds., Cenozoic Basins of the Death Valley Region: Geological Society of America Special Paper 333, p. 65-86.

Christiansen, R.L., Lipman, P.W., Carr, W.J., Byers, F.M., Jr., Orkild, P.P., and Sargent, K.A., 1977, The Timber Mountain–Oasis Valley caldera complex of southern Nevada: Geological Society of America Bulletin, v. 88, p. 943-959.

Crowe, B., Perry, F., Geissman, J., McFadden, L., Wells, S., Murrell, M., Poths, J., Valentine, G.A., Bowker, L., and Finnegan, K., 1995, Status of volcanism studies for the Yucca Mountain site characterization project: Los Alamos National Laboratory Report LA-12908-MS, 379 p.

Fridrich, C.J., 1999, Tectonic evolution of the Crater Flat basin, Yucca Mountain region, Nevada, *in* Wright, L. A., and Troxel, B. W., editors, Cenozoic Basins of the Death Valley Region: Geological Society of America Special Paper 333, Boulder, Colorado, Geological Society of America, p. 169-195.

Harris, R.N., Ponce, D.A., Healey, D.L., and Oliver, H.W., 1989, Principal facts for about 16,000 gravity stations in the Nevada Test Site and vicinity: U.S. Geological Survey Open-File Report 89-682A, 78 p.

Hayford, J.F., and Bowie, William, 1912, The effect of topography and isostatic compensation upon the intensity of gravity: U.S Coast and Geodetic Survey Special Publication 10, 132 p.

Heiskanen, W.A., and Vening Meinesz, F.A., 1958, The Earth and its Gravity Field: New York, McGraw-Hill, 470 p.

Hildenbrand, T.G., 1983, FFTFIL: A filtering program based on two-dimensional Fourier analysis: U.S. Geological Survey Open-File Report 83-237, 61 p.

Hillhouse, J.W., and Morin, Robert, 2003, Investigation of linear magnetic anomalies in the Funeral Mountains, Death Valley region, California: U.S. Geological Survey Open-File Report 2003-12, 16 p.

Jachens, R.C., and Moring, B.C., 1990, Maps of the thickness of Cenozoic deposits and the isostatic residual gravity over basement for Nevada: U.S. Geological Survey Open-File Report 90-404, 15 p.

Langenheim, V.E., 1995, Magnetic and gravity studies of buried volcanic centers in the Amargosa Desert and Crater Flat, southwest Nevada: U.S. Geological Survey Open-File Report 95-564, 37 p.

Langenheim, V.E., Kirchoff-Stein, K.S., and Oliver, H.W., 1993, Geophysical investigations of buried volcanic centers near Yucca Mountain, southwest Nevada: Proceedings, Fourth International Conference, High Level Radioactive Waste Management, Las Vegas, Nevada, v. 2, p. 1840-1846.

Mankinen, E.A., Hildenbrand, T.G., Fridrich, C.J., McKee, E.H., and Schenkel, C.J., 2003, Geophysical setting of the Pahute Mesa–Oasis Valley region, southern Nevada: Nevada Bureau Mines and Geology Report 50, CD-ROM, 45 p.

Morelli, C., ed., 1974, The International Gravity Standardization Net 1971: International Association of Geodesy Special Publication 4, 194 p.

O'Leary, D.W., Mankinen, E.A., Blakely, R.J., Langenheim, V.E., and Ponce, D.A., 2002, Aeromagnetic expression of buried basaltic volcanoes near Yucca Mountain, Nevada: U.S. Geological Survey Open-File Report 02-020, 48 p.

Perry, F.V., Cogbill, A.H., and Kelley, R.E., 2005, Uncovering Buried Volcanoes at Yucca Mountain: Eos, v. 86, no. 47, p. 485 and 488.

Peters, L.J., 1949, The direct approach to magnetic interpretation and its practical application: Geophysics, v. 14, p. 290-320.

Plouff, Donald, 1977, Preliminary documentation for a FORTRAN program to compute gravity terrain corrections based on topography digitized on a geographic grid: U.S. Geological Survey Open-File Report 77-535, 45 p.

Ponce, D.A., and Oliver, H.W., 1981, Charleston Peak gravity calibration loop, Nevada: U.S. Geological Survey Open-File Report 81-985, 20 p.

Potter, C.J., Dickerson, R.P., Sweetkind, D.S., Drake, R.M., II, San Juan, C.A., Fridrich, C.J. and Day, W.C., 2002, Geologic map of the Yucca Mountain region: U.S. Geological Survey Miscellaneous Investigations Map I-2755, scale 1:50,000, 2 plates with pamphlet.

Potter, C.J., Sweetkind, D.S., Dickerson, R.P., and M.L. Kilgore, 2002, Hydrostructural maps of the Death Valley regional flow system, Nevada and California: U.S. Geological Survey Miscellaneous Field Studies Map MF-2372, scale 1:350,000.

Sawyer, D.A., Fleck, R.J., Lanphere, M.A., Warren, R.G., Broxton, D.E., and Hudson, M.R., 1994, Episodic caldera volcanism in the Miocene southwestern Nevada volcanic field: Revised stratigraphic framework, $^{40}Ar/^{39}Ar$ geochronology, and implications for magmatism and extension: Geological Society of America Bulletin, v. 106, p. 1304-1318.

Simpson, R.W., Jachens, R.C., and Blakely, R.J., 1983, Airyroot: a FORTRAN program for calculating the gravitational attraction of an Airy isostatic root out to 166.7 km: U.S. Geological Survey Open-File Report 83-883, 66 p.

Simpson, R.W., Jachens, R.C., Blakely, R.J., and Saltus, R.W., 1986, A new isostatic residual gravity of the conterminous United States, with a discussion of the significance of the isostatic residual anomalies: Journal of Geophysical Research, v. 91, p. 8348-8372.

Spielman, J.B., and Ponce, D.A., 1984, HANDTC, a FORTRAN program to calculate inner-zone terrain corrections: U.S. Geological Survey Open-File Report 84-777, 20 p.

Stewart, J.H., 1988, Tectonics of the Walker Lane belt, western Great Basin Mesozoic and Cenozoic deformation in a zone of shear, *in* Ernst, W.G., ed., Metamorphism and crustal evolution of the western United States (Ruby Volume 7): Englewood Cliffs, N.J., Prentice-Hall, p. 683–713.

Stewart, J.H., and Crowell, J.C., 1992, Strike-slip tectonics in the Cordillera region, western United States, *in* Burchfiel, B.C., Lipman, P.W., and Zoback, M.L., eds., The Cordilleran orogen in conterminous U.S.: Geological Society of America, Geology of North America, v. H–3, p. 609–628.

Sweetkind, D.S., Fridrich, C.J., and Taylor, E., 2001a, Facies analysis of Tertiary basin-filling rocks of the Death Valley regional ground-water system and surrounding areas, Nevada and California: U.S. Geological Survey Open-File Report 01-400, 55 p.

Sweetkind, D.S., Dickerson, R.P., Blakely, R.J., and Denning, P.D., 2001b, Interpretive geologic cross sections for the Death Valley regional flow system and surrounding areas, Nevada and California: U.S. Geological Survey Miscellaneous Field Studies Map MF–2370, 3 sheets.

Walker, G.E., and Eakin, T.E., 1963, Geology and ground water of Amargosa Desert, Nevada-California: State of Nevada Department of Conservation and Natural Resources Reconnaissance Series Report 14, 45 p.

Webring, M., 1985, SAKI-FORTRAN program for generalized linear inversion of gravity and magnetic profiles: U.S. Geological Survey Open-File Report 85-122, 29 p.

Workman, J.B., Menges, C.M., Page, W.R., Taylor, E.M., Ekren, E.B., Rowley, P.D., Dixon, G.L., Thompson, R.A., and Wright, L.A., 2002, Geologic map of the Death Valley ground-water model area, Nevada and California: U.S. Geological Survey Miscellaneous Field Studies Map MF–2381–A, scale 1:250,000.

Wright, L.A., 1989, Overview of the role of strike-slip and normal faulting in the Neogene history of the region northeast of Death Valley, California–Nevada, *in* Ellis, M.A., ed., Late Cenozoic evolution of the southern Great Basin: Nevada Bureau of Mines and Geology Open-File Report 89–1, Selected papers from a workshop at University of Nevada, Reno, November 10–13, 1987, p. 1–11.

Wright, L.A., Thompson, R.A., Troxel, B.W., Pavlis, T.L., DeWitt, E., Otton, J.K., Ellis, M.A., Miller, M.G., and Serpa, L.F., 1991, Cenozoic magmatic and tectonic evolution of the east-central Death Valley region, California, *in* Walawender, M.J., and Hanan, B.B., eds., Geological excursions in southern California and Mexico: Geological Society of America, Geological Society of America Annual Meeting Guidebook 1991, p. 93-127.

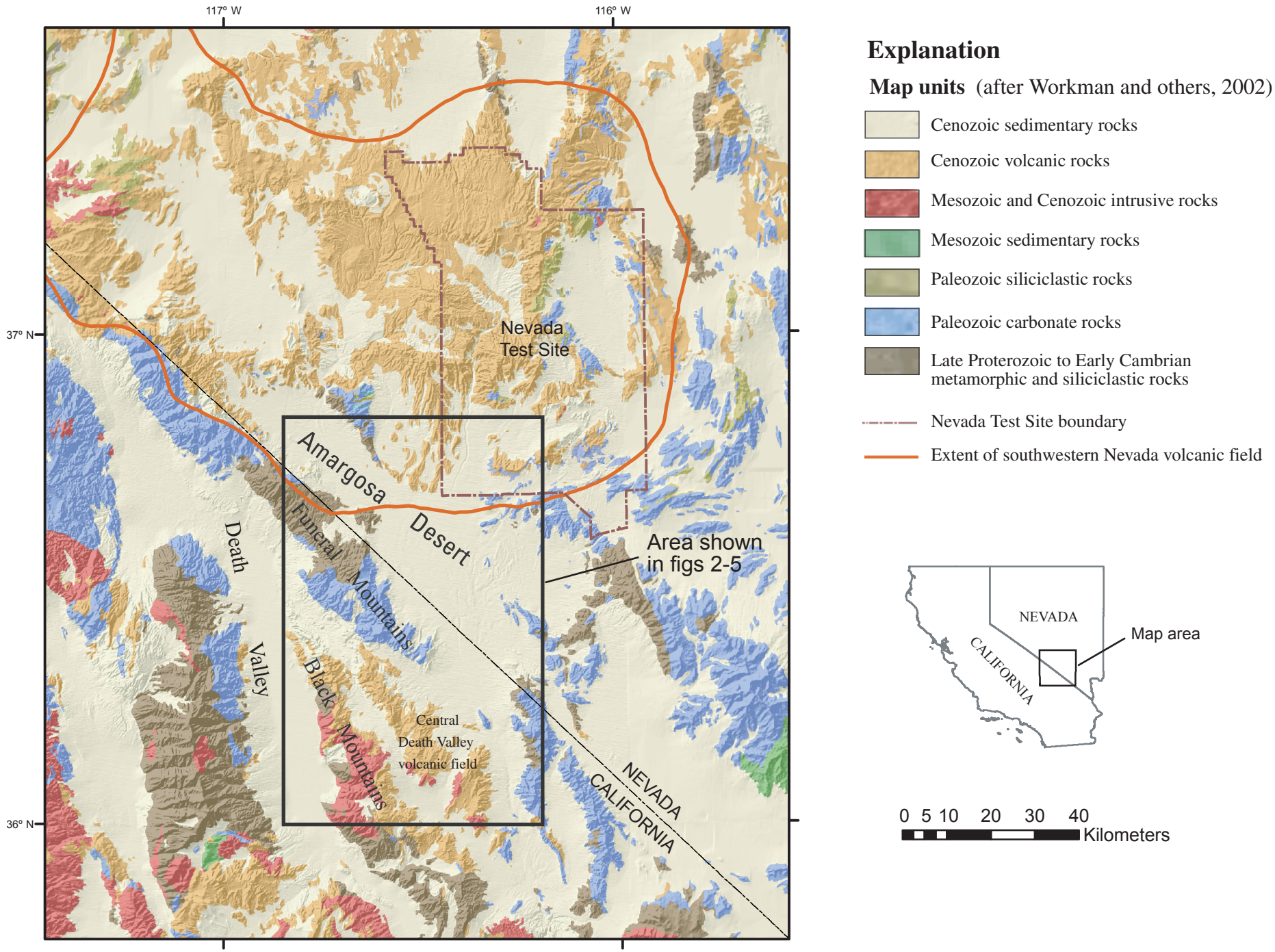

Figure 1. Index map showing location of Amargosa Desert basin study area (outlined) and distribution of main geologic units of the surrounding region.

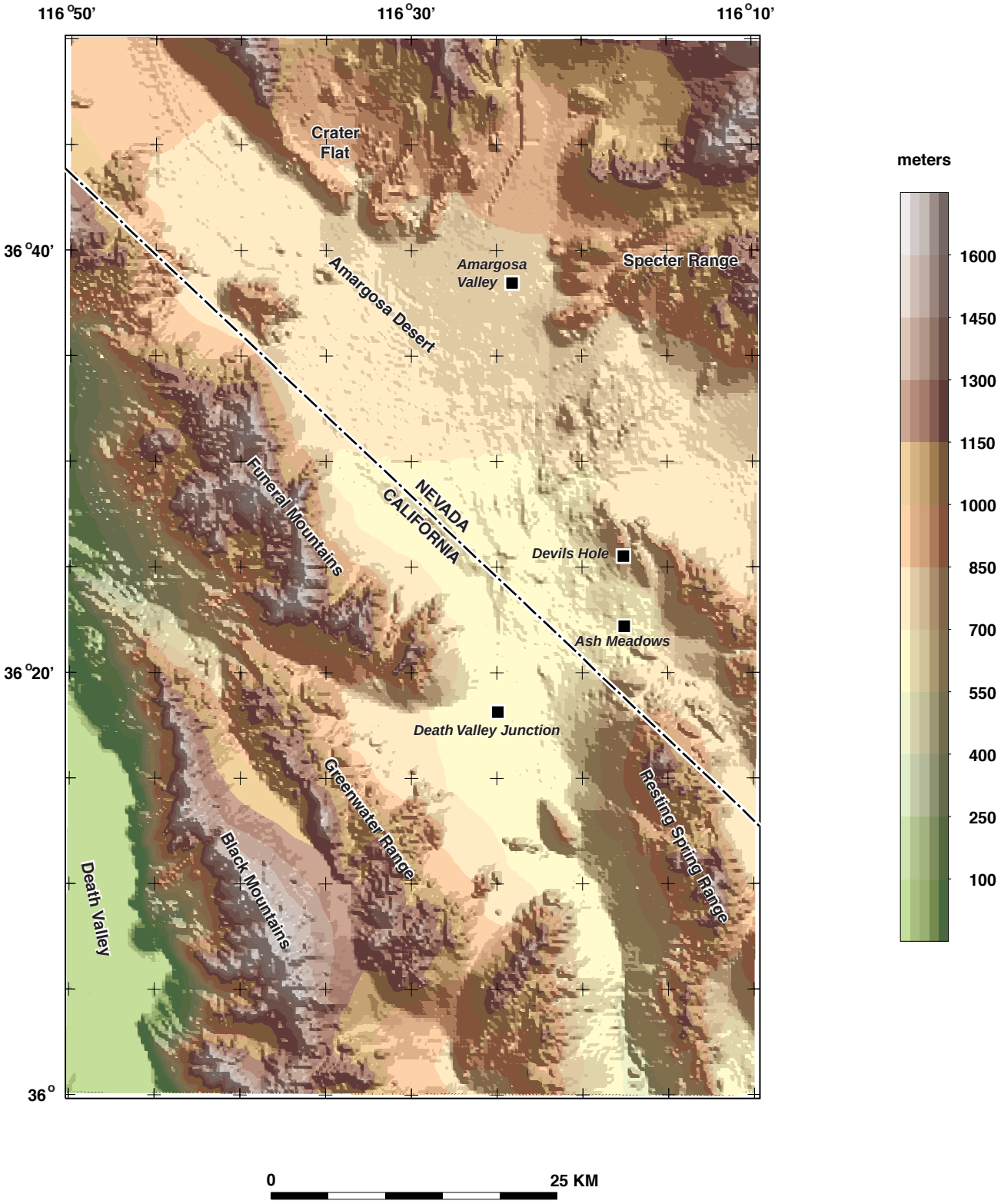

Figure 2. Map showing location of Amargosa Desert basin study area.

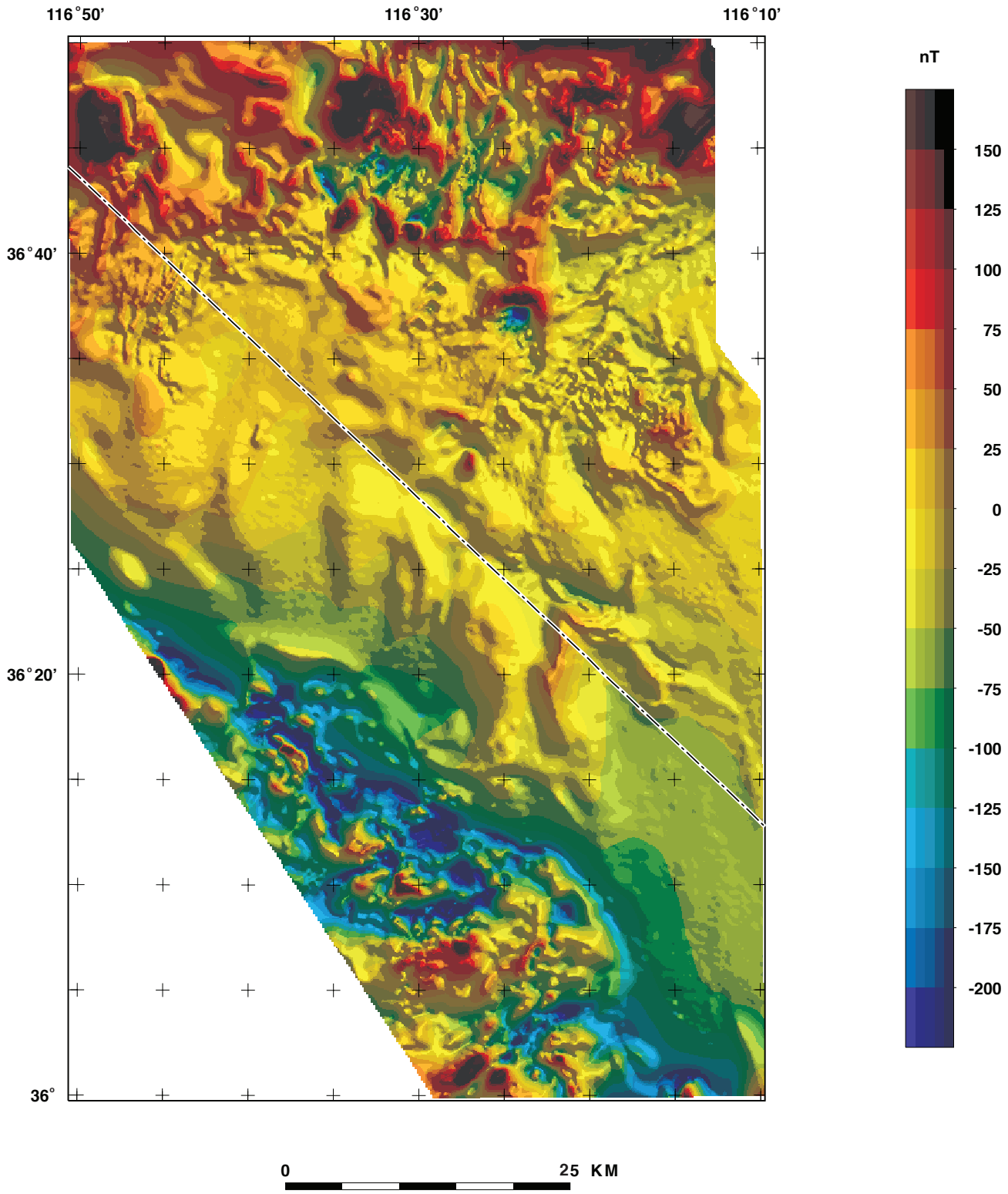

Figure 3. Magnetic anomalies over parts of the study area shown in figures 1 & 2, extracted from the high-resolution aeromagnetic survey of Blakely and others (2000). Colors represent measured magnetic field intensities relative to the International Geomagnetic Reference Field.

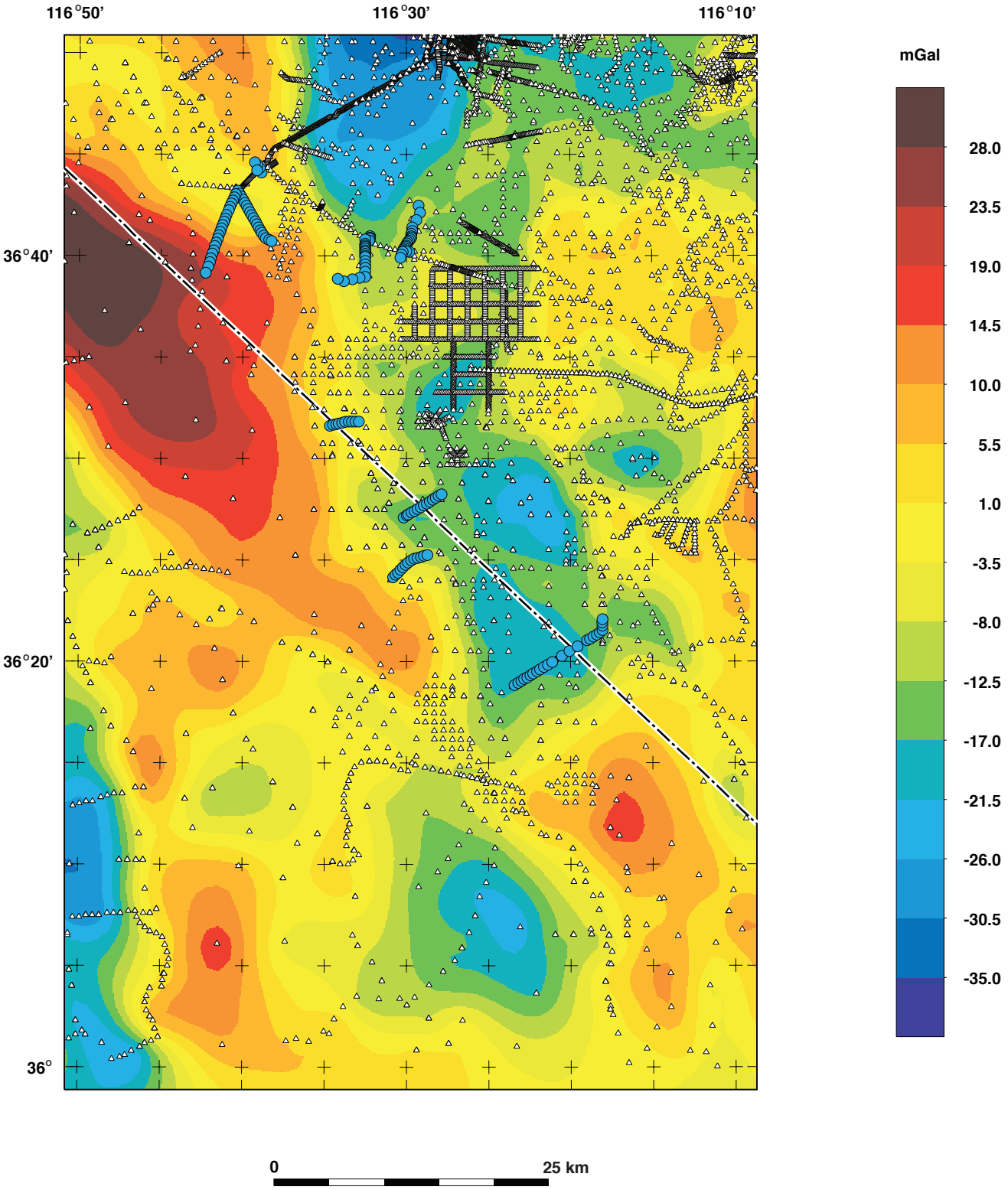

Figure 4. Isostatic residual gravity map of the Amargosa Desert basin area showing locations of previously available gravity stations (triangles) and those established during this study (circles).

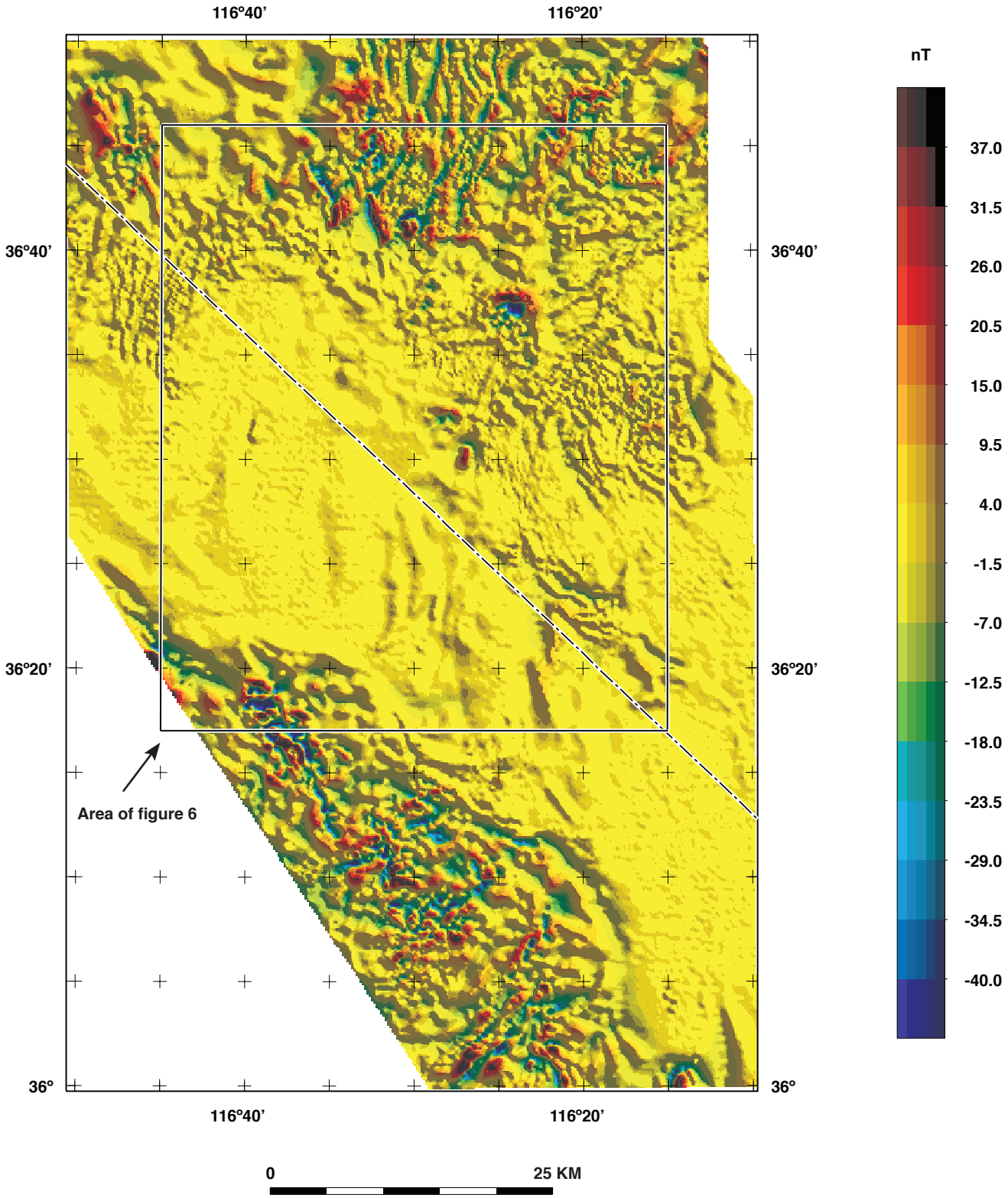

Figure 5. Residual magnetic anomalies over parts of the study area shown in figures 1 & 2, modified from Blakely and others (2000). Data shown in figure 3 have been reprocessed to emphasize surface and near-surface sources (see text).

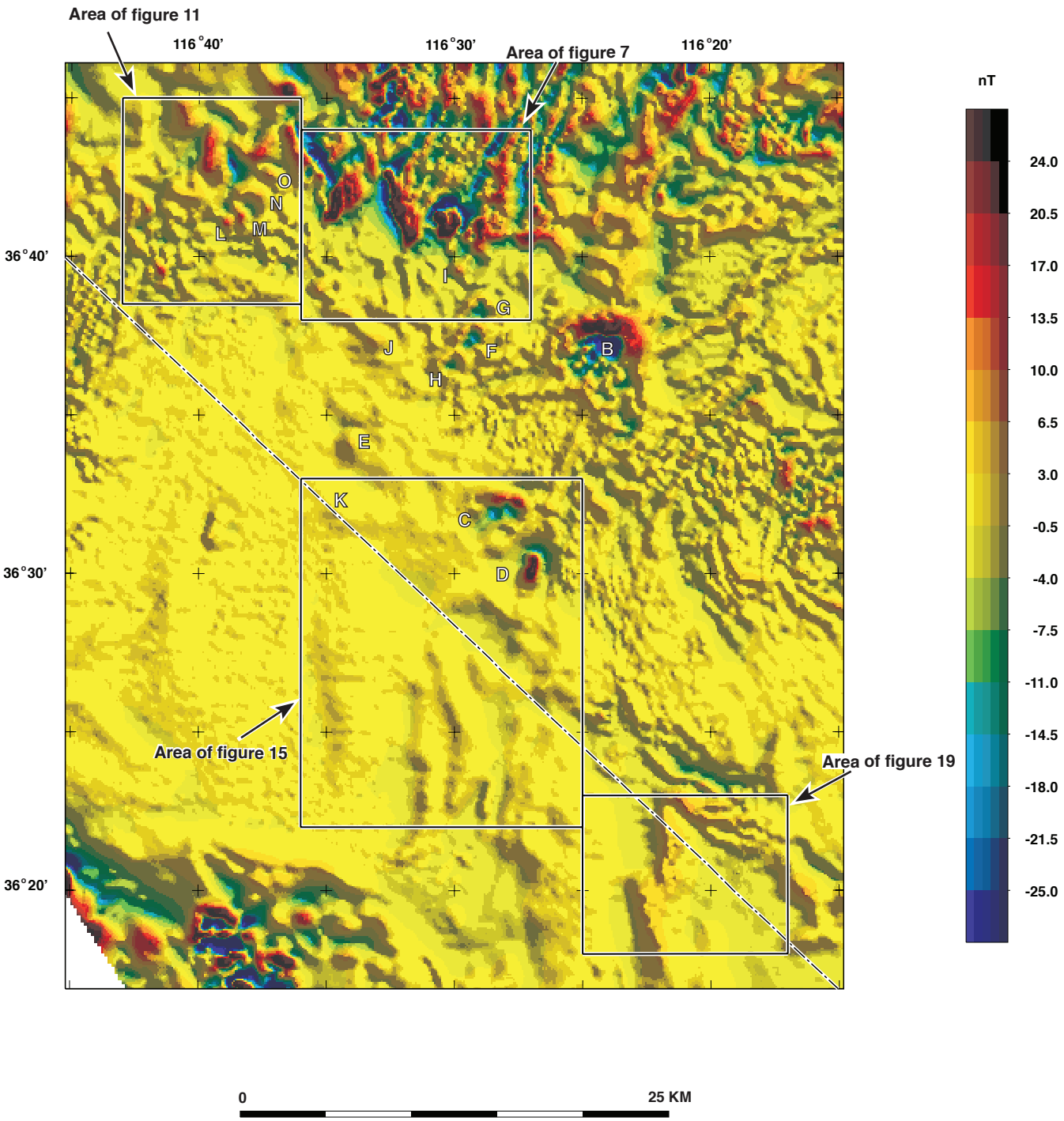

Figure 6. Portion of residual magnetic anomaly map shown in figure 5. Labeled anomalies reflect sources buried beneath alluvial fill (O'Leary and others, 2002).

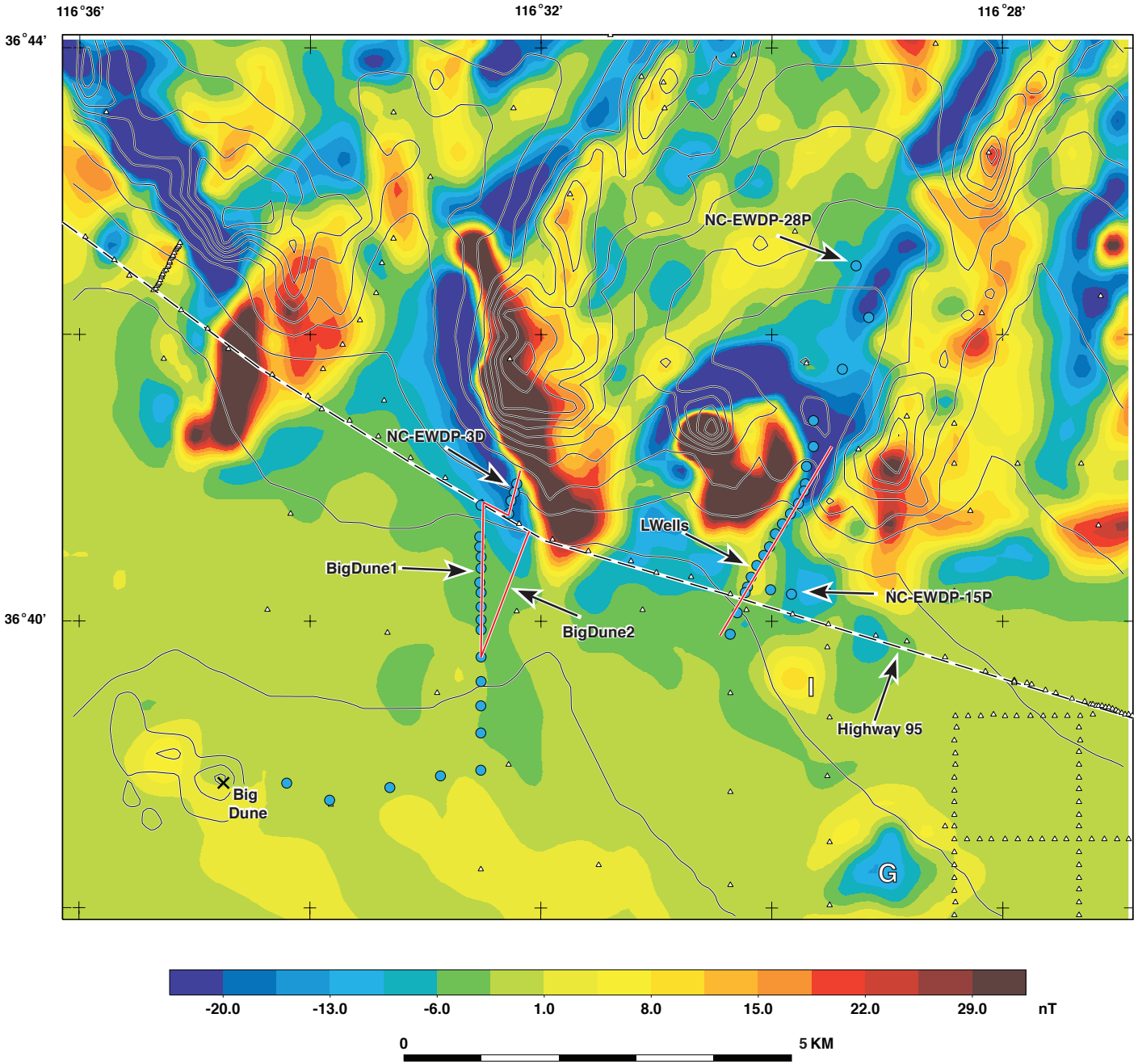

Figure 7. Portion of residual magnetic map of figure 6 showing locations of detailed gravity and ground magnetic profiles (red lines) in the vicinity of highway 95. Also shown are locations of some Nye County Early Warning Drilling Program (NC-EWDP) boreholes. Topographic contour interval = 20 m. See figures 3 and 6 for additional explanation.

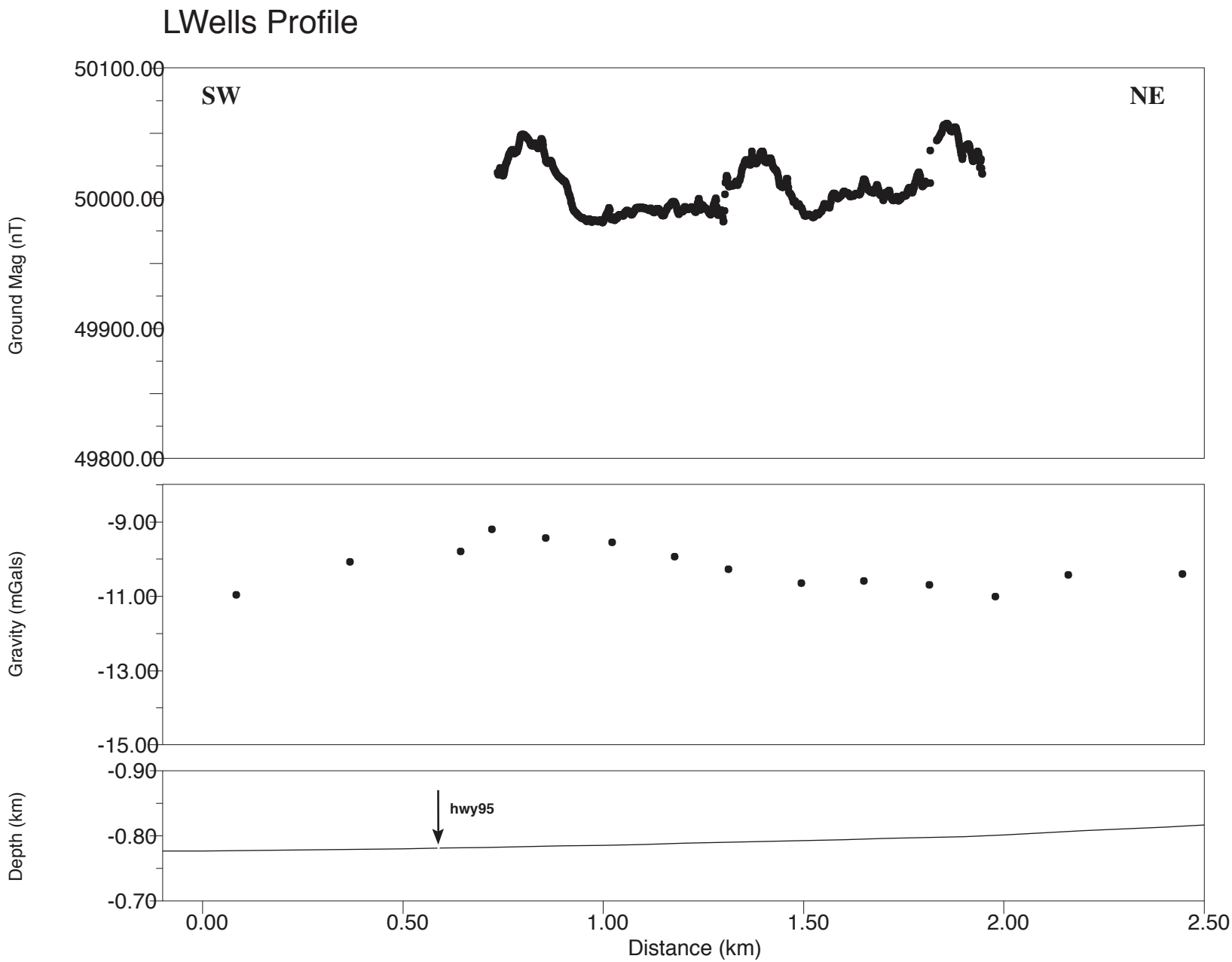

Figure 8. Gravity and ground magnetic profiles along profile "LWells" shown in figure 7.

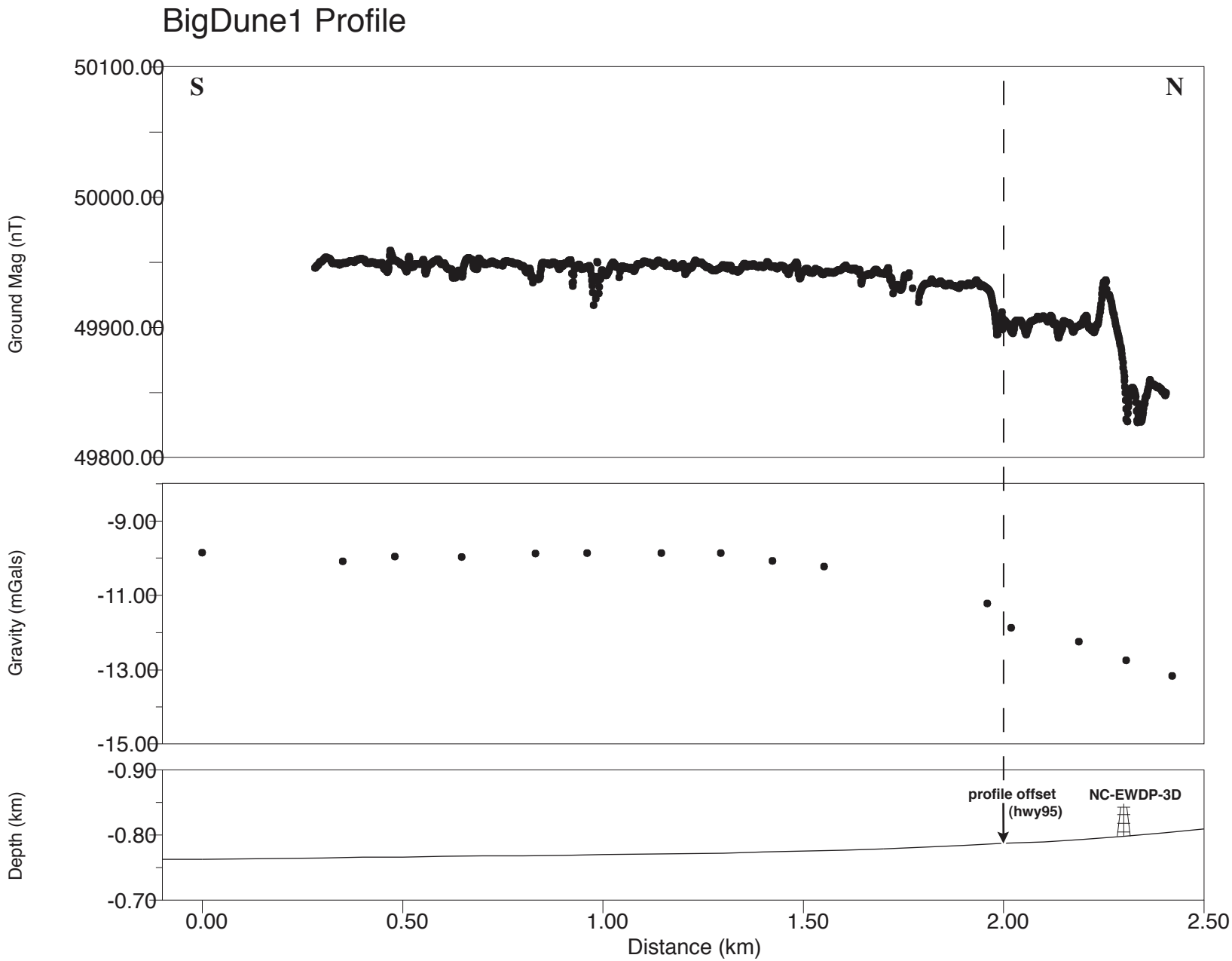

Figure 9. Gravity and ground magnetic profiles along profile "BigDune1" shown in figure 7.

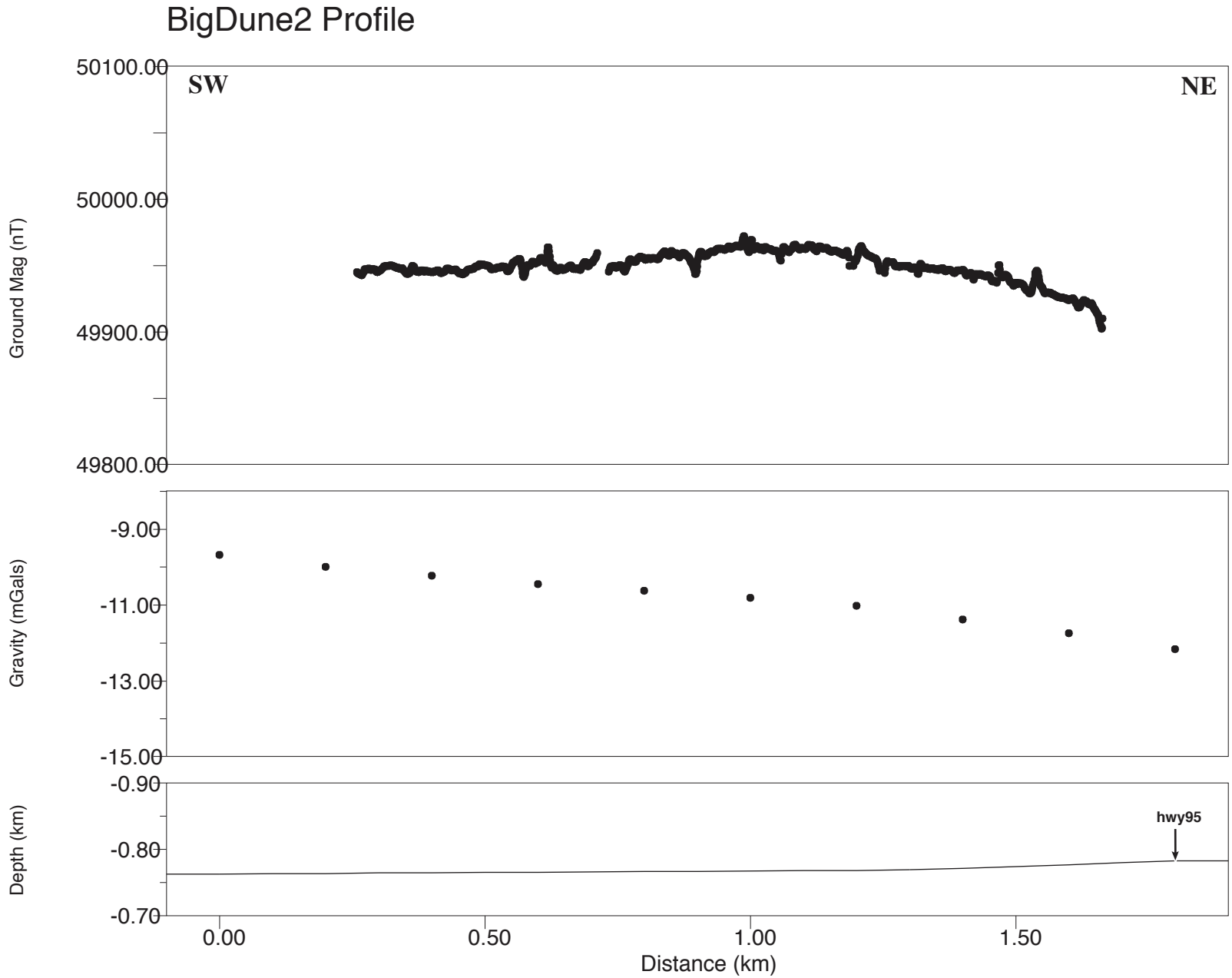

Figure 10. Gravity and ground magnetic profiles along profile "BigDune2" shown in figure 7.

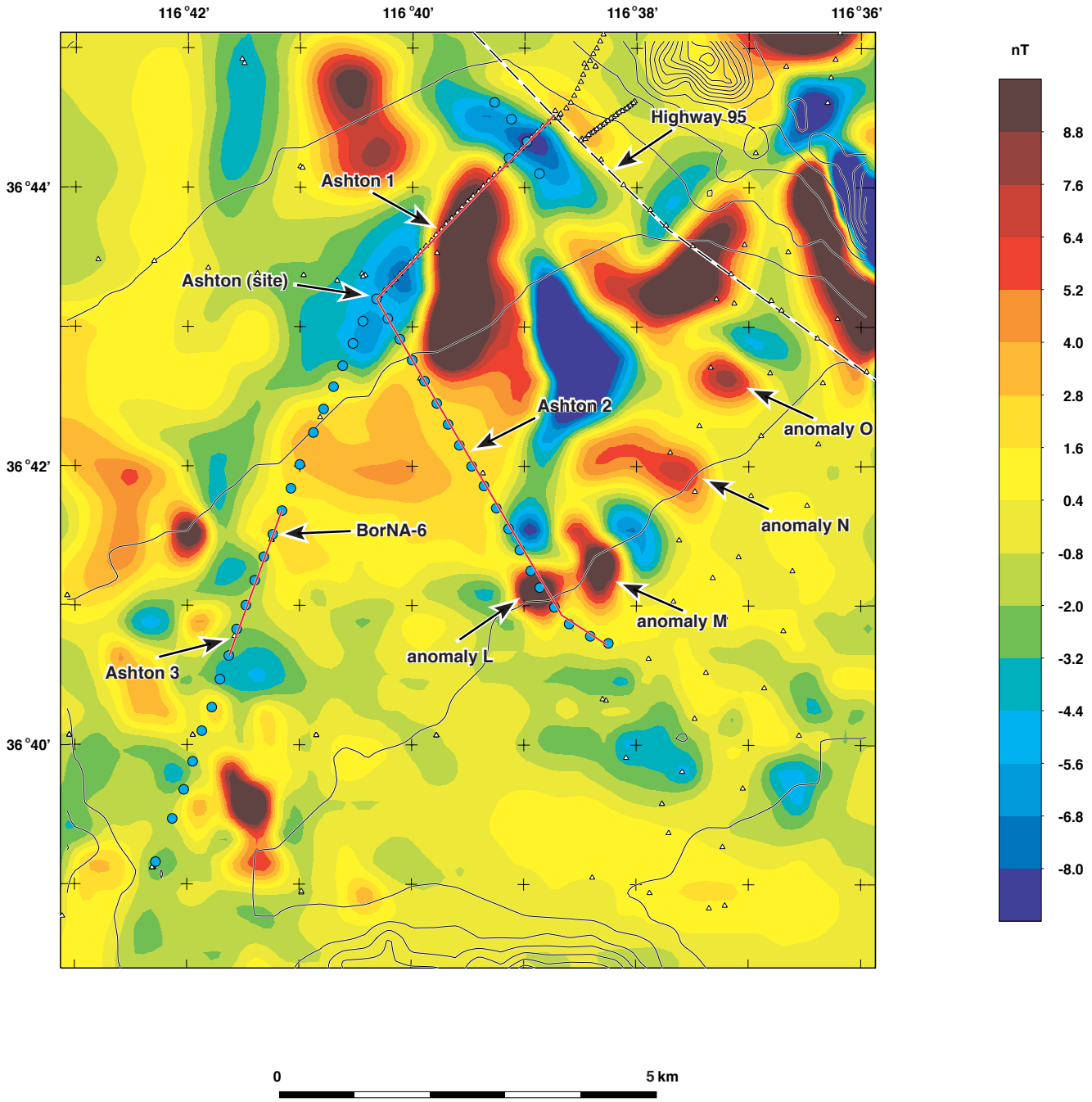

Figure 11. Portion of residual magnetic map of figure 6 showing locations of detailed gravity and ground magnetic profiles in the Ashton vicinity. Also shown is the location of U.S. Borax borehole, BorNA-6. See figures 3, 6, and 7 for additional explanation.

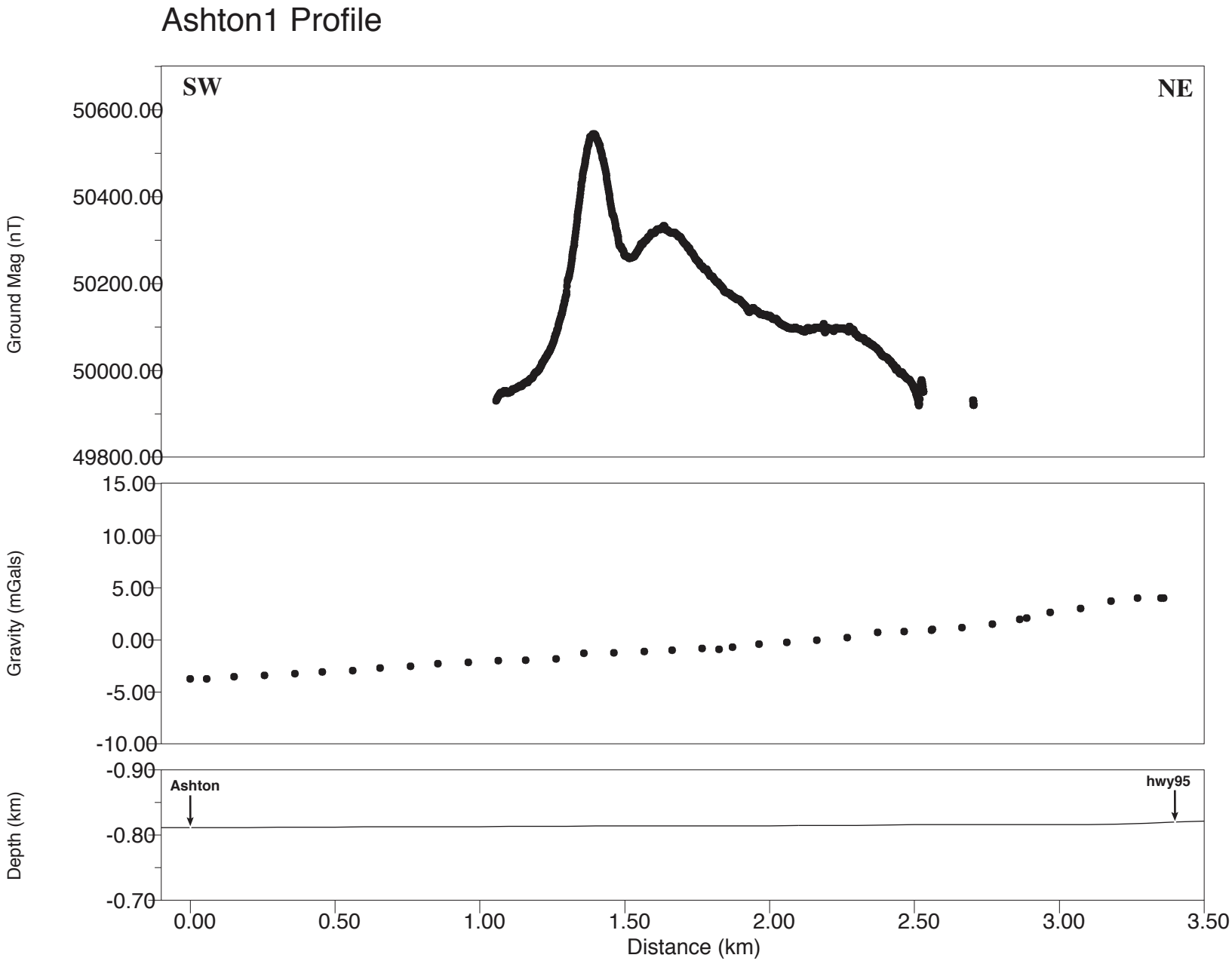

Figure 12. Gravity and ground magnetic profiles along profile "Ashton1" shown in figure 11.

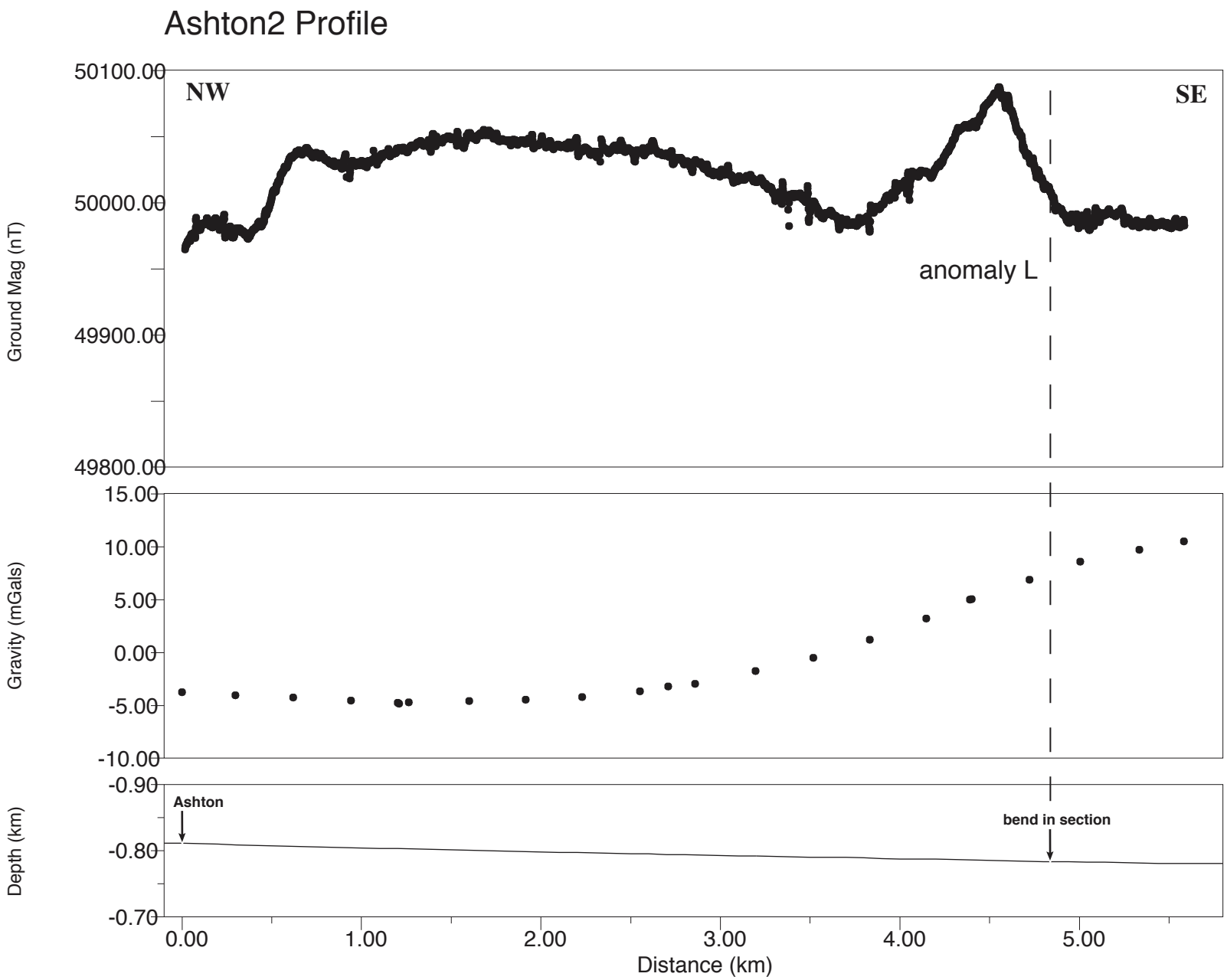

Figure 13. Gravity and ground magnetic profiles along profile "Ashton2" shown in figure 11.

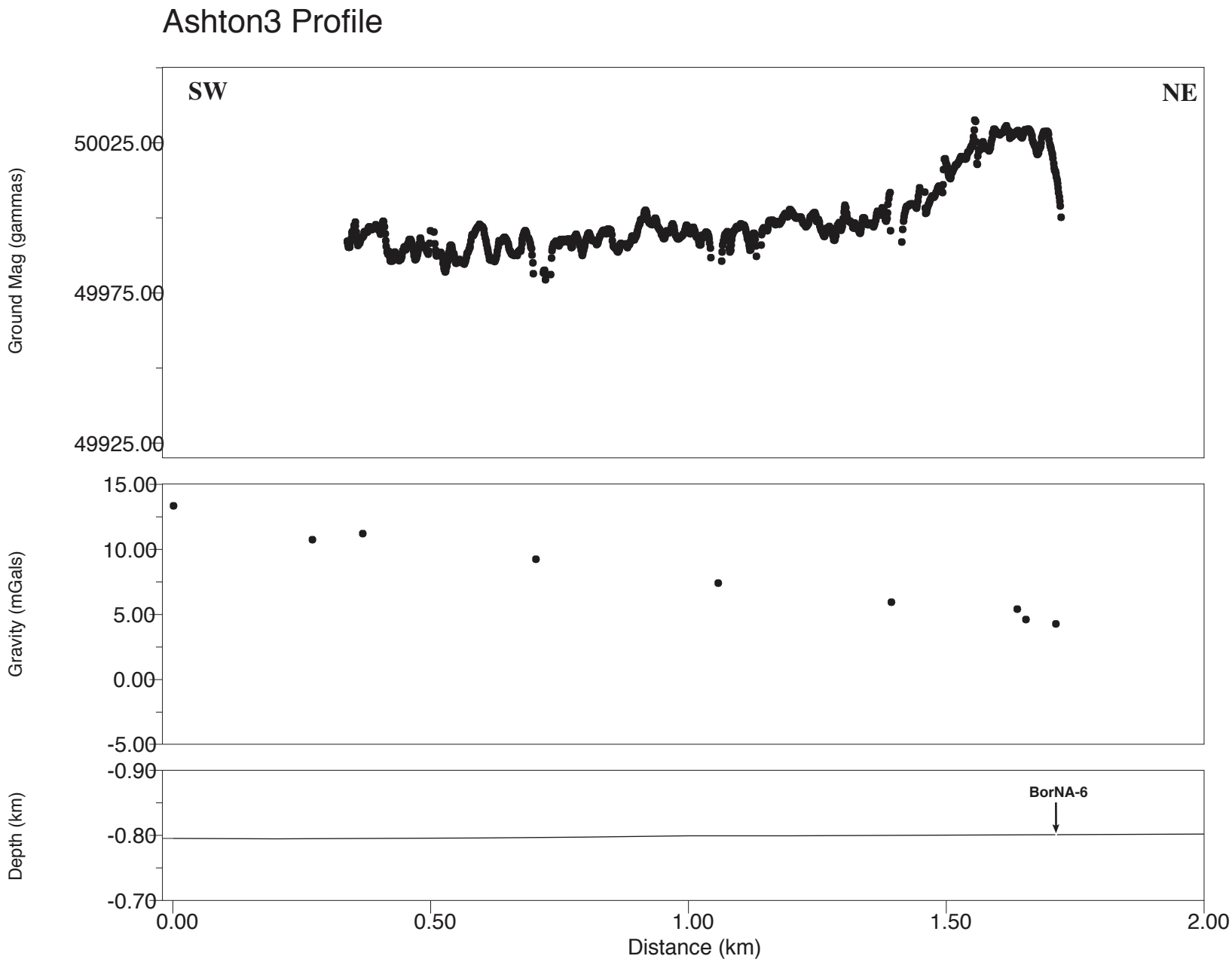

Figure 14. Gravity and ground magnetic profiles along profile "Ashton3" shown in figure 11.

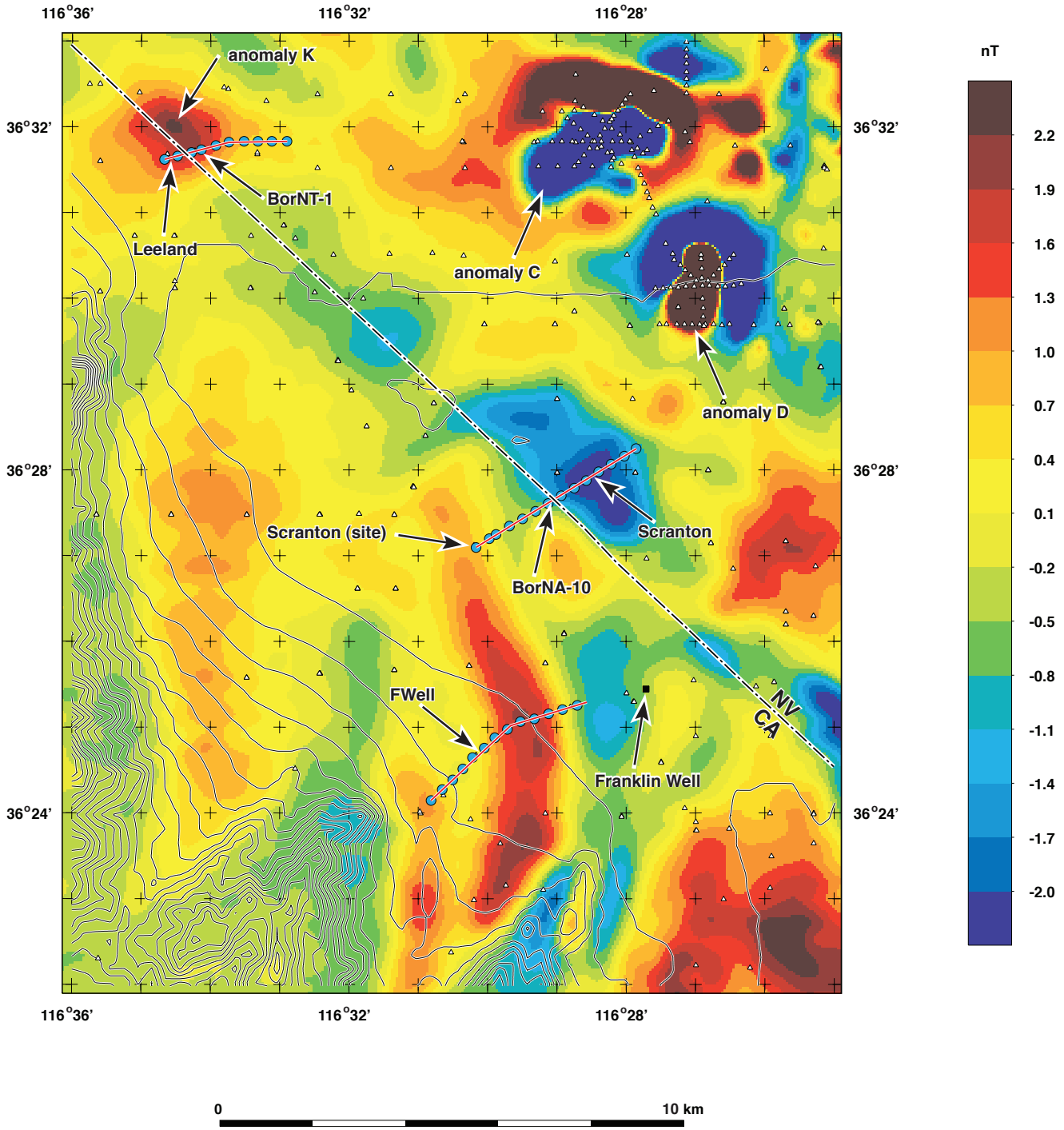

Figure 15. Portion of residual magnetic map of figure 6 showing locations of detailed gravity and ground magnetic profiles northeast of the Funeral Mountains. Also shown are the locations of U.S. Borax boreholes, BorNT-1 and BorNA-10. Topographic contour interval = 50 m.

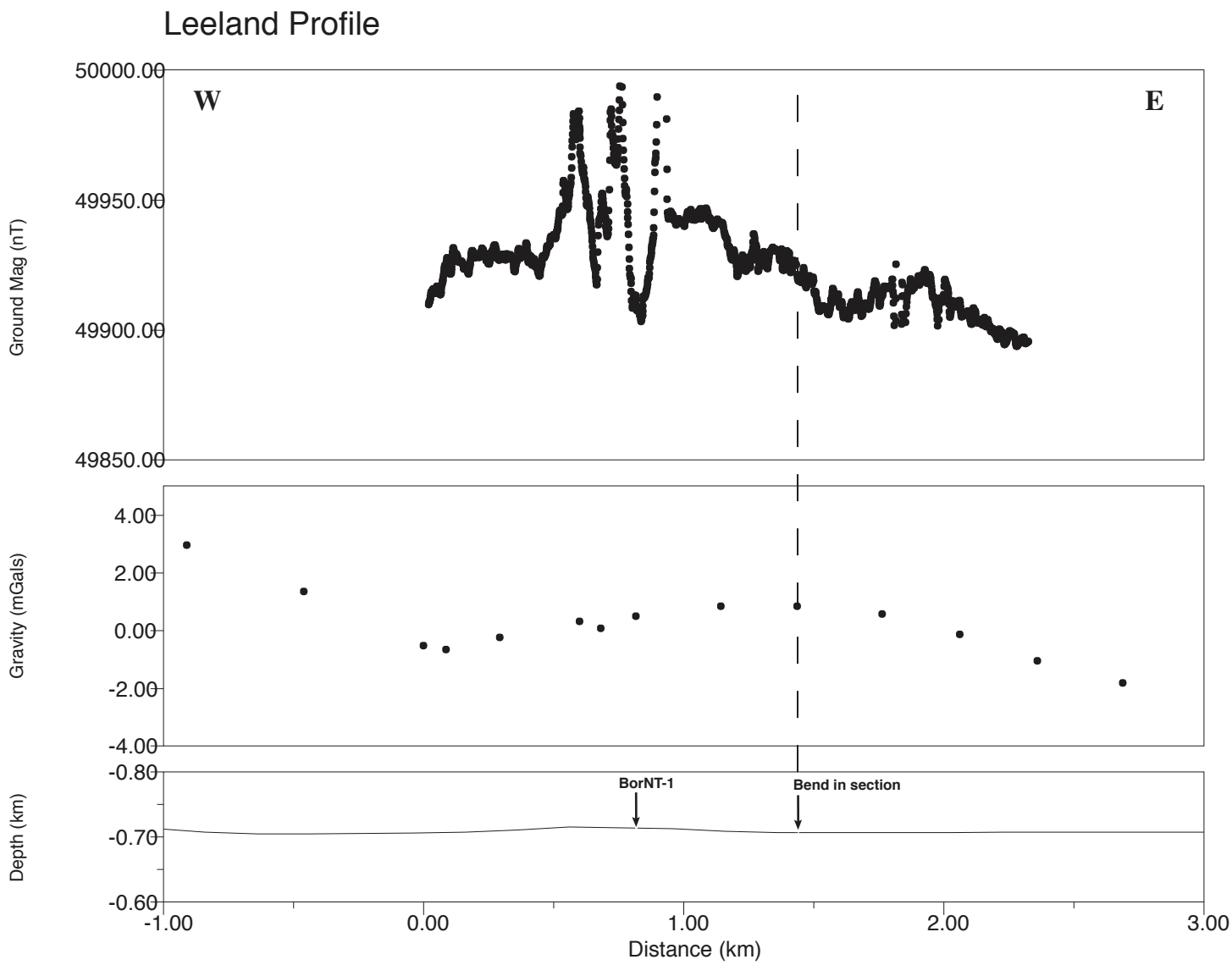

Figure 16. Gravity and ground magnetic profiles along profile "Leeland" shown in figure 15.

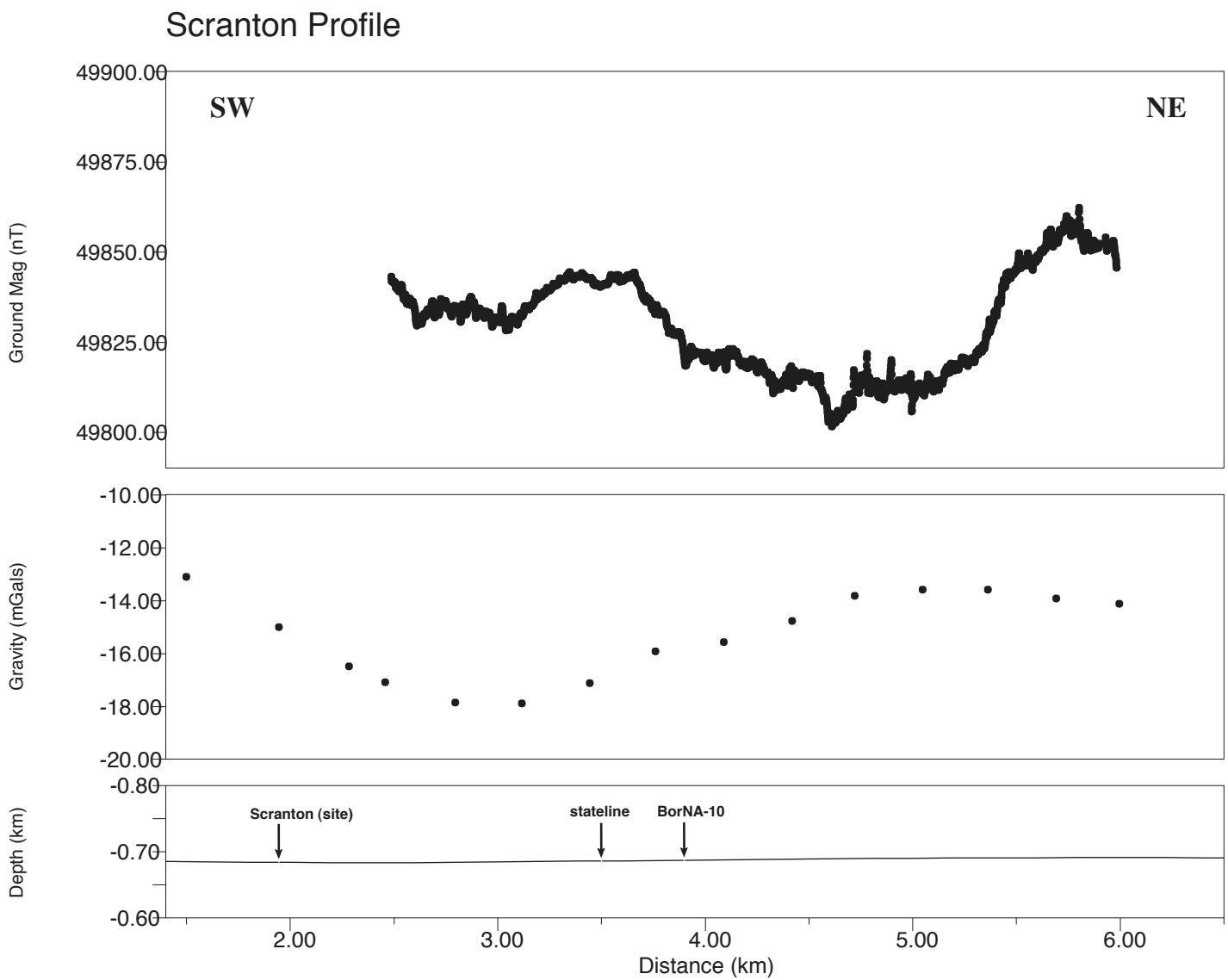

Figure 17. Gravity and ground magnetic profiles along profile "Scranton" shown in figure 15.

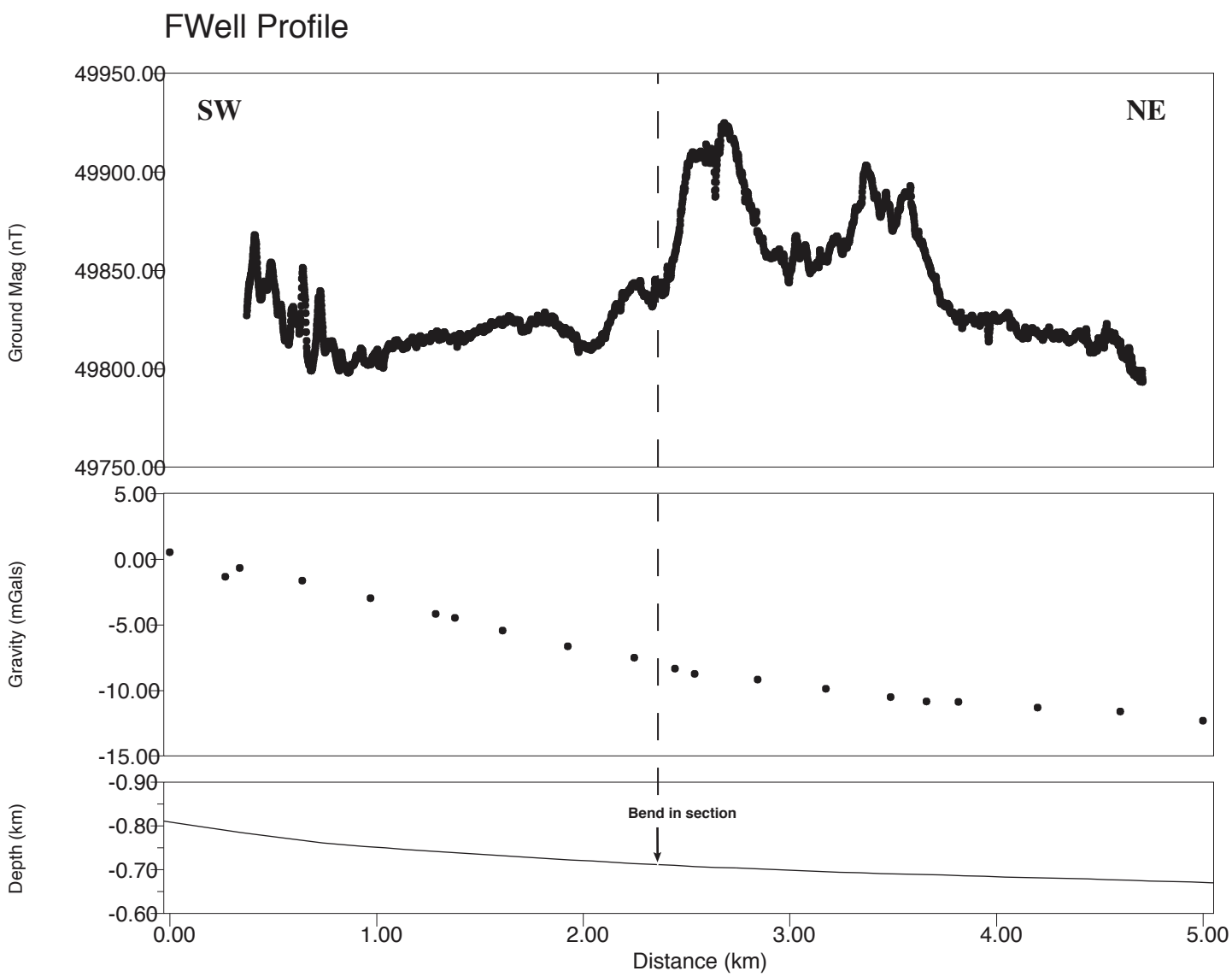

Figure 18. Gravity and ground magnetic profiles along profile "FWell" shown in figure 15.

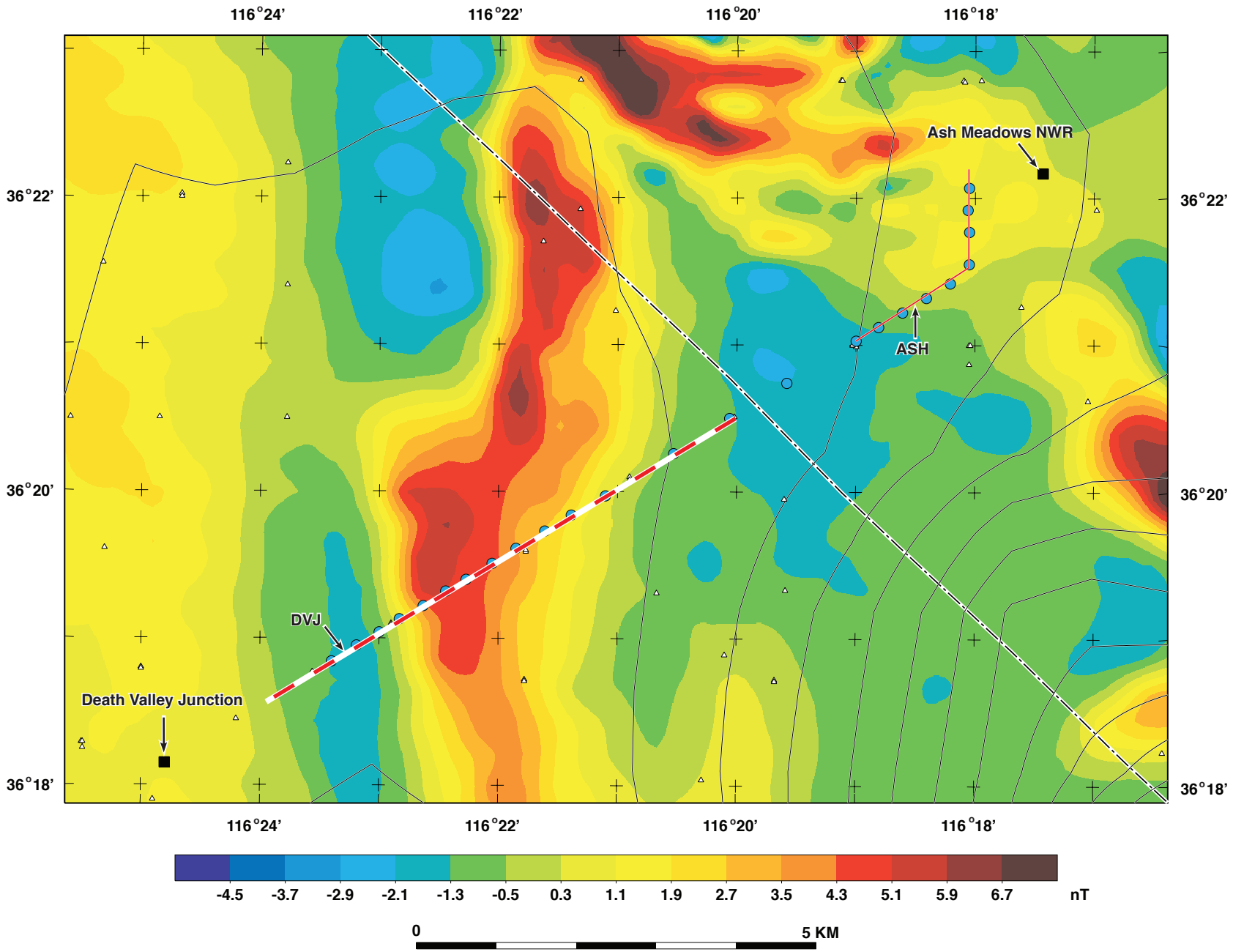

Figure 19. Portion of residual magnetic map of figure 6 showing location of detailed gravity and ground magnetic profiles in the vicinity of Death Valley Junction. Dashed red/white line is profile DVJ from Blakely and others (2005). Topographic contour interval = 20 m.

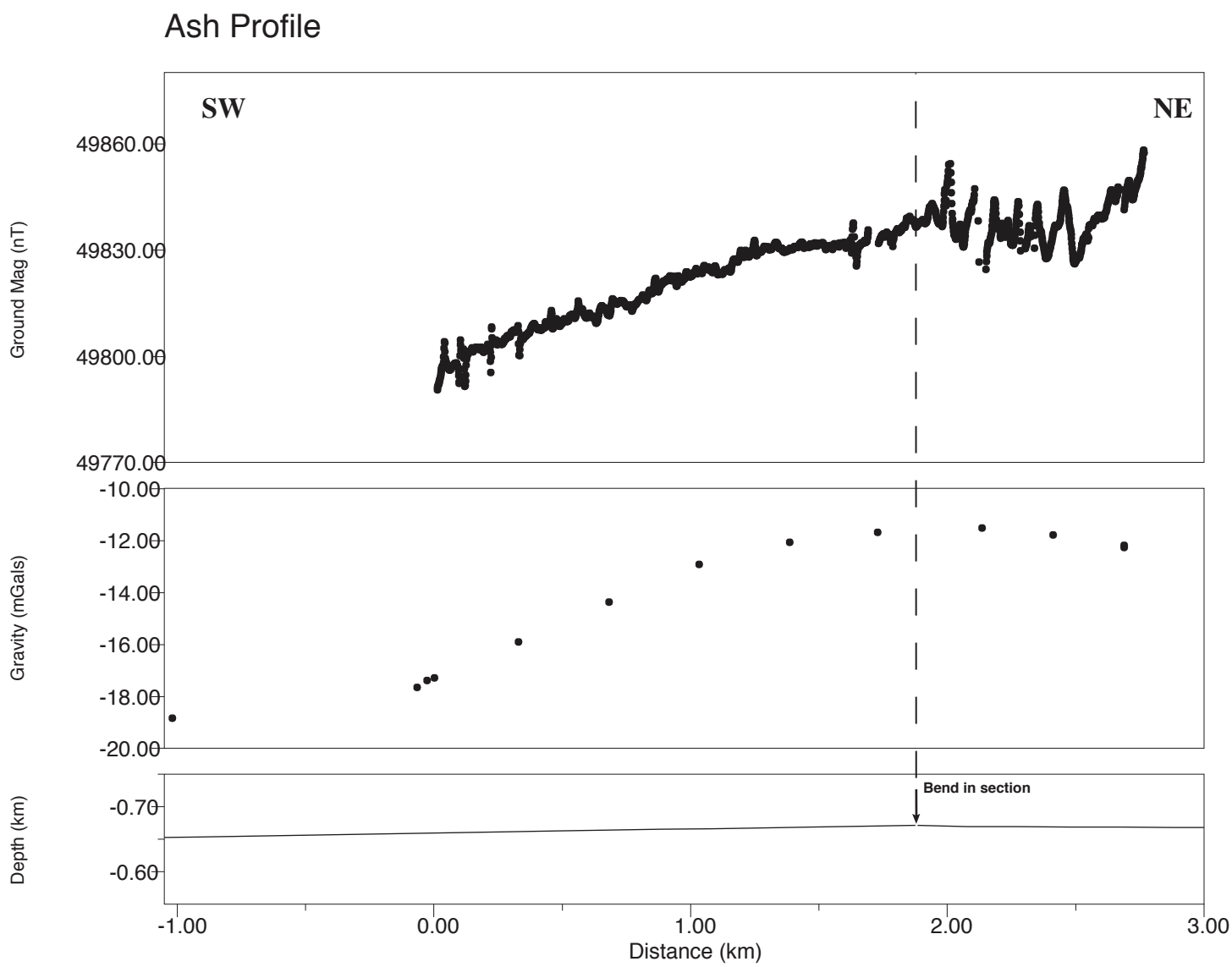

Figure 20. Gravity and ground magnetic profiles along profile "Ash" shown in figure 19.

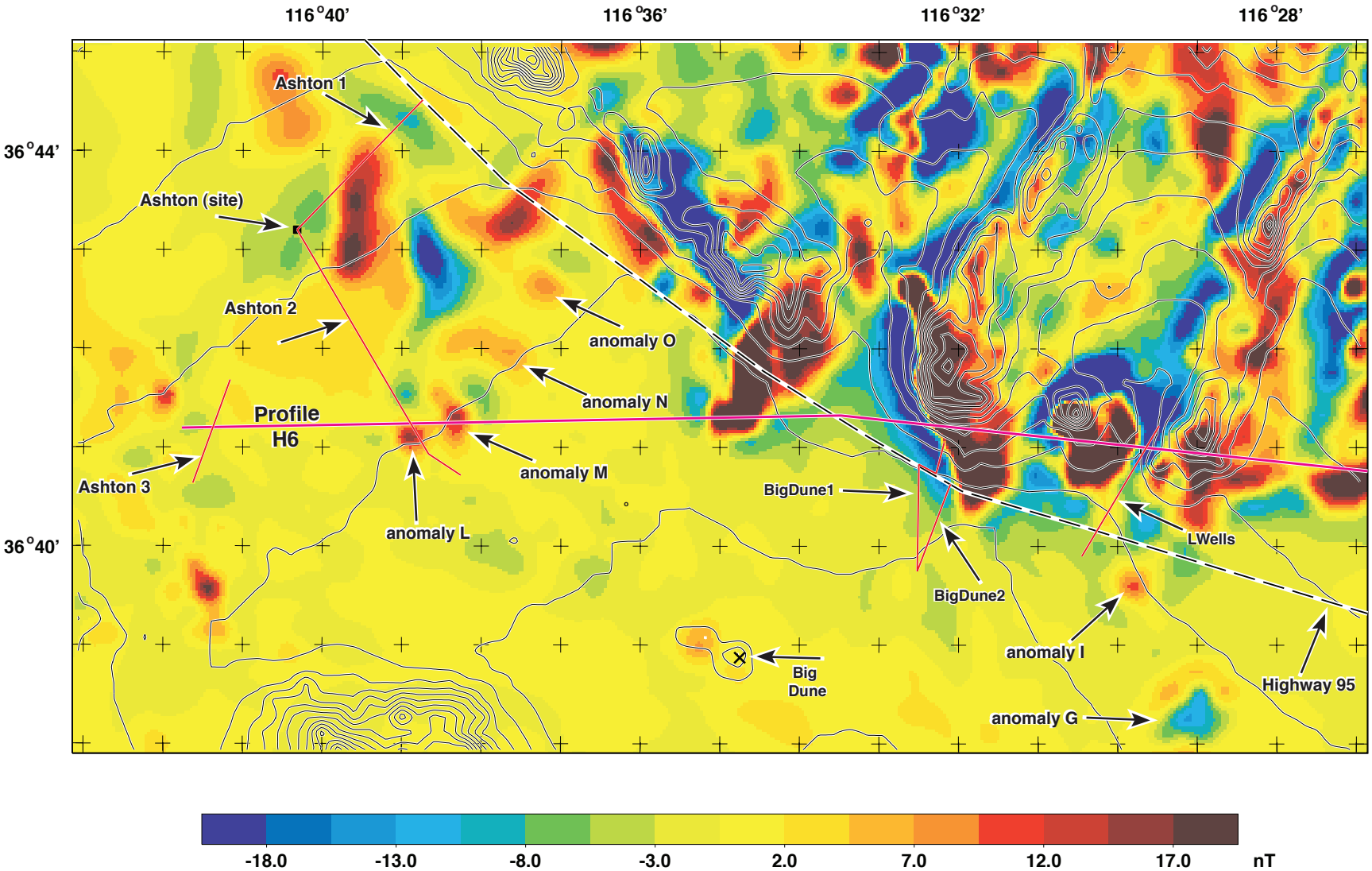

Figure 21. Portion of residual magnetic map of figure 5 showing locations of ground magnetic profiles in the Ashton to Lathrop Wells vicinity. Also shown is the location of geologic cross-section H6 of Sweetkind and others (2001). Topographic contour interval = 20 m.

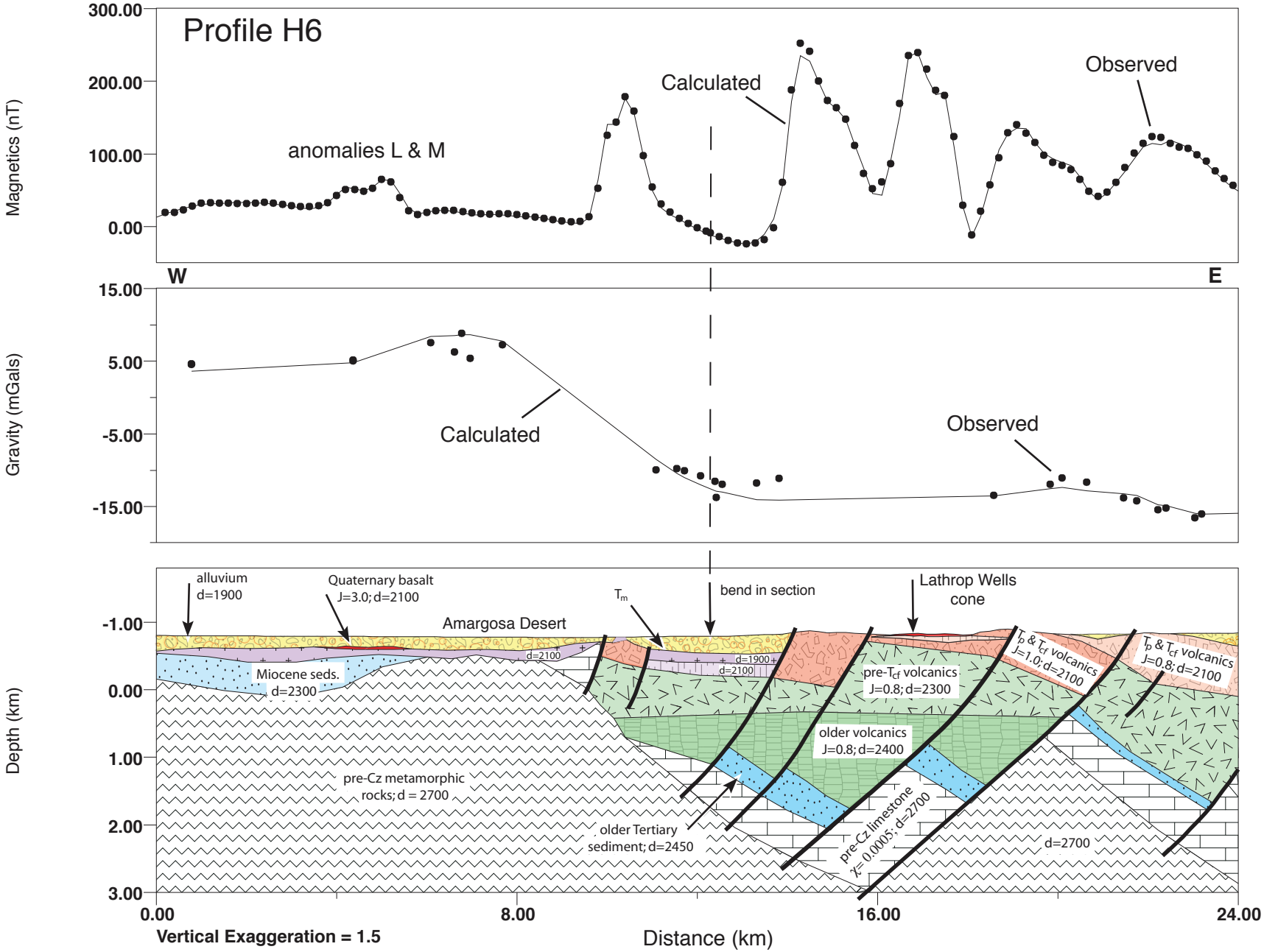

Figure 22. Geophysical forward model showing fits between observed and calculated magnetic and gravity profiles, and a geologic interpretation of inferred subsurface structure using geologic cross-section H6 (Sweetkind and others, 2001) as a guide. J, magnetization (A/m); d, density (kg/m^3); χ, susceptibility (SIU). T_m, Timber Mountain Group; T_p, Paintbrush Group; T_{cf}, Crater Flat Group.

TABLE 1. — ***Principal facts of gravity stations from Amargosa Desert Basin***

STATION NAME	LATITUDE	LONGITUDE	ELEV (m)	OBS GRAV (mGal)	FREE AIR	TERRAIN HAND	TERRAIN TOT	BOUG ANOM	ISOST ANOM
03AM001	36 42.48	116 29.27	861.1	979581.16	-32.6	0.2D	0.5	-129.5	-7.9
03AM002	36 42.12	116 29.16	849.4	979584.55	-32.3	0.2D	0.4	-127.9	-6.8
03AM003	36 41.76	116 29.39	838.8	979586.93	-32.7	0.2D	0.4	-127.1	-6.4
03AM004	36 41.40	116 29.64	828.0	979589.19	-33.2	0.1D	0.4	-126.5	-6.3
03AM005	36 41.22	116 29.64	824.1	979588.94	-34.4	0.1D	0.4	-127.2	-7.2
03AM006	36 41.08	116 29.70	821.2	979589.09	-34.9	0.1D	0.4	-127.4	-7.6
03AM007	36 40.96	116 29.71	819.2	979589.22	-35.3	0.2D	0.4	-127.5	-7.8
03AM008	36 40.91	116 29.72	804.7	979589.44	-39.5	0.1D	0.4	-130.0	-10.4
03AM009	36 40.82	116 29.77	798.6	979590.07	-40.6	0.1D	0.4	-130.5	-11.0
03AM010	36 40.75	116 29.84	797.1	979590.75	-40.3	0.1D	0.3	-130.0	-10.7
03AM011	36 40.68	116 29.91	794.9	979591.31	-40.2	0.0D	0.3	-129.8	-10.6
03AM012	36 40.61	116 29.97	791.9	979591.84	-40.6	0.0D	0.3	-129.8	-10.6
03AM013	36 40.52	116 30.02	791.0	979592.41	-40.2	0.0D	0.3	-129.3	-10.3
03AM014	36 40.46	116 30.07	790.0	979592.90	-39.8	0.0D	0.3	-128.9	-9.9
03AM015	36 40.39	116 30.13	788.8	979593.55	-39.5	0.0D	0.2	-128.4	-9.6
03AM016	36 40.31	116 30.18	786.4	979594.15	-39.5	0.0D	0.2	-128.2	-9.4
03AM017	36 40.24	116 30.21	785.2	979594.61	-39.3	0.0D	0.2	-127.9	-9.2
03AM018	36 40.19	116 29.83	786.7	979594.71	-38.7	0.0D	0.2	-127.4	-8.7
03AM019	36 40.22	116 30.01	783.9	979596.08	-38.2	0.0D	0.2	-126.6	-7.9
03AM020	36 40.20	116 30.23	781.6	979594.70	-40.3	0.0D	0.2	-128.4	-9.8
03AM021	36 40.06	116 30.30	779.7	979594.81	-40.5	0.0D	0.2	-128.5	-10.1
03AM022	36 39.91	116 30.36	778.5	979594.15	-41.4	0.0D	0.2	-129.2	-11.0
03AM023	36 40.96	116 32.21	805.2	979587.16	-41.6	0.1D	0.5	-132.2	-13.2
03AM024	36 40.90	116 32.23	798.5	979588.93	-41.9	0.1D	0.4	-131.7	-12.8
03AM025	36 40.84	116 32.26	792.3	979590.65	-41.9	0.1D	0.4	-131.1	-12.2
03AM026	36 40.75	116 32.28	785.2	979592.44	-42.2	0.1D	0.4	-130.6	-11.9
03AM027	36 40.81	116 32.52	784.3	979593.38	-41.7	0.0D	0.4	-130.0	-11.2
03AM028	36 40.59	116 32.53	774.3	979596.29	-41.5	0.0D	0.3	-128.7	-10.2
03AM029	36 40.52	116 32.53	773.9	979596.52	-41.3	0.0D	0.3	-128.5	-10.1
03AM030	36 40.45	116 32.52	772.2	979597.05	-41.2	0.0D	0.3	-128.2	-9.9
03AM031	36 40.37	116 32.52	771.8	979597.14	-41.1	0.0D	0.3	-128.1	-9.9
03AM032	36 40.27	116 32.53	770.7	979597.32	-41.1	0.0D	0.3	-128.0	-9.9
03AM033	36 40.20	116 32.52	769.4	979597.56	-41.2	0.0D	0.2	-127.9	-9.9
03AM034	36 40.10	116 32.52	768.3	979597.67	-41.3	0.0D	0.2	-127.9	-10.0
03AM035	36 40.01	116 32.52	767.0	979597.90	-41.3	0.0D	0.2	-127.8	-10.0
03AM036	36 39.94	116 32.52	766.0	979597.97	-41.5	0.0D	0.2	-127.8	-10.1
03AM037	36 39.75	116 32.52	763.6	979598.60	-41.3	0.0D	0.2	-127.4	-9.9
03AM038	36 39.58	116 32.52	761.7	979599.29	-40.9	0.0D	0.2	-126.8	-9.5
03AM039	36 39.41	116 32.52	759.5	979600.04	-40.6	0.0D	0.2	-126.3	-9.1
03AM040	36 39.22	116 32.52	756.8	979600.73	-40.5	0.0D	0.2	-125.9	-8.9
03AM041	36 38.96	116 32.52	754.2	979601.18	-40.5	0.0D	0.2	-125.6	-8.9
03AM042	36 38.92	116 32.87	754.8	979601.51	-39.9	0.0D	0.2	-125.1	-8.5
03AM043	36 38.84	116 33.31	753.3	979602.76	-39.0	0.0D	0.2	-124.0	-7.7
03AM044	36 38.75	116 33.83	751.9	979604.76	-37.3	0.0D	0.2	-122.1	-6.0
03AM045	36 38.87	116 34.20	753.2	979606.39	-35.4	0.0D	0.2	-120.4	-4.2
03AM046	36 44.10	116 38.87	813.1	979601.11	-29.8	0.0D	0.5	-121.2	0.1
03AM047	36 44.33	116 38.98	815.6	979602.64	-27.8	0.0D	0.5	-119.5	2.1
03AM048	36 44.49	116 39.12	818.0	979602.87	-27.1	0.0D	0.6	-119.0	2.8
03AM049	36 44.61	116 39.27	820.0	979603.09	-26.4	0.0D	0.6	-118.6	3.4
03AM050	36 44.21	116 39.14	815.6	979601.62	-28.6	0.0D	0.5	-120.4	1.0
03AM051	36 43.20	116 40.32	812.0	979597.78	-32.2	0.0D	0.4	-123.6	-3.7
03AM052	36 43.06	116 40.22	809.5	979597.91	-32.6	0.0D	0.4	-123.8	-4.0
03AM053	36 42.91	116 40.11	806.9	979598.19	-32.9	0.0D	0.4	-123.8	-4.2
03AM054	36 42.76	116 40.00	805.1	979598.17	-33.2	0.0D	0.4	-123.9	-4.6
03AM055	36 42.61	116 39.89	803.2	979598.36	-33.4	0.0D	0.3	-123.9	-4.7
03AM056	36 42.45	116 39.78	801.3	979598.79	-33.3	0.0D	0.3	-123.6	-4.6
03AM057	36 42.30	116 39.68	799.5	979599.23	-33.2	0.0D	0.3	-123.3	-4.5
03AM058	36 42.15	116 39.58	797.5	979599.83	-33.1	0.0D	0.3	-122.9	-4.2
03AM059	36 42.00	116 39.47	795.7	979600.67	-32.5	0.0D	0.3	-122.2	-3.7
03AM060	36 41.86	116 39.36	794.2	979601.70	-31.8	0.0D	0.3	-121.3	-3.0

TABLE 1. — ***Principal facts of gravity stations from Amargosa Desert (continued)***

STATION NAME	LATITUDE	LONGITUDE	ELEV (m)	OBS GRAV (mGal)	FREE AIR	TERRAIN HAND	TERRAIN TOT	BOUG ANOM	ISOST ANOM
03AM061	36 41.70	116 39.25	792.0	979603.26	-30.7	0.0D	0.3	-119.9	-1.7
03AM062	36 41.55	116 39.14	790.3	979604.79	-29.4	0.0D	0.3	-118.5	-0.5
03AM063	36 41.40	116 39.04	789.0	979606.72	-27.7	0.0D	0.3	-116.6	1.2
03AM064	36 41.25	116 38.94	787.6	979608.93	-25.7	0.0D	0.3	-114.5	3.2
03AM065	36 41.13	116 38.86	786.4	979610.96	-23.9	0.0D	0.3	-112.5	5.1
03AM066	36 40.99	116 38.73	783.8	979613.21	-22.2	0.0D	0.3	-110.6	6.9
03AM067	36 40.87	116 38.60	782.2	979615.13	-20.6	0.0D	0.3	-108.8	8.6
03AM068	36 40.78	116 38.41	781.6	979616.30	-19.5	0.0D	0.3	-107.6	9.7
03AM069	36 40.73	116 38.25	780.5	979617.29	-18.8	0.0D	0.3	-106.8	10.5
03AM070	36 43.04	116 40.44	809.5	979598.06	-32.4	0.0D	0.4	-123.6	-4.0
03AM071	36 42.88	116 40.53	808.5	979598.07	-32.5	0.0D	0.4	-123.5	-4.1
03AM072	36 42.72	116 40.62	807.5	979598.35	-32.3	0.0D	0.4	-123.2	-4.0
03AM073	36 42.57	116 40.70	807.1	979598.60	-31.9	0.0D	0.4	-122.8	-3.8
03AM074	36 42.41	116 40.79	805.9	979599.49	-31.2	0.0D	0.4	-121.9	-3.2
03AM075	36 42.24	116 40.88	805.0	979600.53	-30.2	0.0D	0.4	-120.8	-2.3
03AM076	36 42.01	116 41.00	803.4	979602.40	-28.5	0.0D	0.4	-118.9	-0.7
03AM077	36 41.84	116 41.08	802.4	979603.89	-27.0	0.0D	0.4	-117.4	0.6
03AM078	36 41.68	116 41.16	802.0	979605.65	-25.2	0.0D	0.4	-115.5	2.3
03AM079	36 41.51	116 41.24	801.0	979607.79	-23.1	0.0D	0.4	-113.3	4.3
03AM080	36 41.35	116 41.32	799.3	979609.78	-21.4	0.0D	0.4	-111.4	5.9
03AM081	36 41.18	116 41.40	798.9	979611.32	-19.7	0.0D	0.4	-109.7	7.4
03AM082	36 41.00	116 41.48	798.2	979613.25	-17.8	0.0D	0.4	-107.6	9.2
03AM083	36 40.83	116 41.56	796.2	979615.60	-15.8	0.0D	0.4	-105.4	11.2
03AM084	36 40.64	116 41.63	796.1	979617.68	-13.5	0.0D	0.4	-103.0	13.3
03AM085	36 40.47	116 41.71	795.8	979619.27	-11.7	0.0D	0.4	-101.2	14.9
03AM086	36 40.27	116 41.78	795.4	979620.11	-10.7	0.0D	0.5	-100.2	15.7
03AM087	36 40.10	116 41.87	794.6	979621.91	-8.9	0.0D	0.5	-98.3	17.4
03AM088	36 39.88	116 41.95	792.0	979623.78	-7.5	0.0D	0.5	-96.6	18.8
03AM089	36 39.68	116 42.03	791.6	979625.15	-6.0	0.0D	0.5	-95.0	20.1
03AM090	36 39.47	116 42.13	789.7	979627.14	-4.3	0.0D	0.6	-93.0	21.8
03AM091	36 39.16	116 42.28	791.7	979628.74	-1.6	0.1D	0.6	-90.5	23.9
03AM092	36 24.15	116 30.82	771.4	979595.58	-19.4	0.1D	1.5	-105.2	0.5
03AM093	36 24.28	116 30.66	761.5	979596.61	-21.6	0.1D	1.3	-106.5	-0.7
03AM094	36 24.39	116 30.51	753.0	979597.52	-23.5	0.1D	1.1	-107.5	-1.6
03AM095	36 24.52	116 30.36	743.6	979598.20	-25.9	0.1D	1.0	-109.0	-3.0
03AM096	36 24.65	116 30.22	734.4	979598.99	-28.1	0.0D	0.9	-110.3	-4.2
03AM097	36 24.76	116 30.05	724.4	979599.80	-30.6	0.0D	0.8	-111.7	-5.4
03AM098	36 24.88	116 29.90	716.0	979600.38	-32.7	0.0D	0.8	-113.0	-6.6
03AM099	36 24.98	116 29.72	708.9	979601.00	-34.5	0.0D	0.7	-113.9	-7.5
03AM100	36 25.07	116 29.53	705.4	979600.54	-36.1	0.1D	0.6	-115.3	-8.8
03AM101	36 25.10	116 29.33	696.9	979601.81	-37.5	0.0D	0.6	-115.8	-9.2
03AM102	36 25.16	116 29.12	692.5	979602.01	-38.8	0.0D	0.6	-116.6	-9.9
03AM103	36 25.21	116 28.92	689.0	979602.10	-39.8	0.0D	0.5	-117.3	-10.5
03AM104	36 25.26	116 28.71	684.8	979602.60	-40.7	0.0D	0.4	-117.7	-10.9
03AM105	36 18.84	116 23.40	623.2	979599.78	-53.3	0.0D	0.4	-123.4	-18.2
03AM106	36 18.95	116 23.19	623.3	979600.36	-52.8	0.0D	0.3	-123.0	-17.7
03AM107	36 19.04	116 23.00	622.4	979600.76	-52.8	0.0D	0.3	-122.9	-17.5
03AM108	36 19.13	116 22.83	621.9	979600.74	-53.1	0.0D	0.4	-123.1	-17.6
03AM109	36 19.22	116 22.63	622.2	979600.76	-53.2	0.0D	0.3	-123.2	-17.6
03AM110	36 19.32	116 22.44	622.4	979601.00	-53.0	0.1D	0.4	-123.1	-17.3
03AM111	36 19.40	116 22.27	623.1	979600.77	-53.2	0.0D	0.3	-123.3	-17.5
03AM112	36 19.51	116 22.05	623.7	979600.53	-53.4	0.1D	0.3	-123.6	-17.6
03AM113	36 19.61	116 21.85	624.2	979600.16	-53.7	0.1D	0.4	-123.9	-17.9
03AM114	36 19.73	116 21.61	625.4	979599.58	-54.1	0.1D	0.3	-124.5	-18.3
03AM115	36 19.84	116 21.39	627.1	979598.80	-54.5	0.1D	0.3	-125.2	-18.8
03AM116	36 19.97	116 21.10	628.7	979598.01	-55.0	0.0D	0.3	-125.8	-19.3
03AM117	36 20.26	116 20.53	639.7	979595.55	-54.5	0.1D	0.3	-126.6	-19.6
03AM118	36 20.50	116 20.06	643.6	979595.16	-54.0	0.0D	0.2	-126.6	-19.3
03AM119	36 20.74	116 19.58	649.9	979594.40	-53.2	0.1D	0.3	-126.4	-18.8
03AM120	36 21.03	116 19.00	662.6	979593.57	-50.5	0.0D	0.2	-125.2	-17.3

TABLE 1. — ***Principal facts of gravity stations from Amargosa Desert (continued)***

STATION NAME	LATITUDE	LONGITUDE	ELEV (m)	OBS GRAV (mGal)	FREE AIR	TERRAIN HAND	TERRAIN TOT	BOUG ANOM	ISOST ANOM
03AM121	36 21.12	116 18.81	665.8	979594.34	-48.9	0.0D	0.2	-124.0	-15.9
03AM122	36 21.22	116 18.61	666.9	979595.64	-47.4	0.0D	0.2	-122.6	-14.4
03AM123	36 21.32	116 18.41	667.9	979596.87	-46.0	0.0D	0.2	-121.3	-12.9
03AM124	36 21.42	116 18.21	668.0	979597.69	-45.3	0.0D	0.3	-120.6	-12.1
03AM125	36 21.55	116 18.05	668.5	979597.96	-45.0	0.0D	0.3	-120.4	-11.7
03AM126	36 21.77	116 18.05	666.9	979598.67	-45.1	0.0D	0.3	-120.3	-11.5
03AM127	36 21.92	116 18.06	666.9	979598.57	-45.4	0.0D	0.2	-120.6	-11.8
03AM128	36 22.07	116 18.05	667.1	979598.26	-45.9	0.0D	0.2	-121.1	-12.2
03AM129	36 31.62	116 34.67	705.8	979614.91	-31.1	0.0D	1.0	-109.9	-0.5
03AM130	36 31.66	116 34.48	709.2	979614.61	-30.4	0.0D	0.9	-109.7	-0.2
03AM131	36 31.70	116 34.28	719.3	979613.18	-28.8	0.1D	0.9	-109.2	0.3
03AM132	36 31.73	116 34.14	711.6	979615.02	-29.4	0.0D	0.8	-109.1	0.5
03AM133	36 31.78	116 33.93	709.1	979615.88	-29.3	0.0D	0.7	-108.8	0.8
03AM134	36 31.82	116 33.74	706.7	979616.35	-29.6	0.0D	0.7	-108.9	0.9
03AM135	36 31.83	116 33.52	706.4	979616.16	-30.0	0.0D	0.6	-109.2	0.6
03AM136	36 31.83	116 33.32	706.5	979615.43	-30.7	0.0D	0.6	-110.0	-0.1
03AM137	36 31.83	116 33.12	707.1	979614.37	-31.5	0.0D	0.5	-111.0	-1.0
03AM138	36 31.83	116 32.90	707.4	979613.51	-32.3	0.0D	0.5	-111.8	-1.8
03AM139	36 27.10	116 30.17	680.3	979601.19	-46.2	0.0D	0.6	-122.5	-15.0
03AM140	36 27.20	116 29.98	679.7	979599.91	-47.8	0.0D	0.5	-124.1	-16.5
03AM141	36 27.25	116 29.88	679.6	979599.36	-48.4	0.0D	0.5	-124.8	-17.1
03AM142	36 27.35	116 29.69	680.3	979598.53	-49.2	0.0D	0.5	-125.7	-17.9
03AM143	36 27.43	116 29.50	684.4	979597.78	-48.8	0.0D	0.4	-125.8	-17.9
03AM144	36 27.52	116 29.31	687.0	979598.12	-47.8	0.0D	0.3	-125.1	-17.1
03AM145	36 27.61	116 29.13	689.5	979598.91	-46.3	0.0D	0.3	-124.0	-15.9
03AM146	36 27.70	116 28.94	692.8	979598.63	-45.7	0.0D	0.3	-123.8	-15.6
03AM147	36 27.79	116 28.75	691.6	979599.72	-45.1	0.0D	0.3	-123.1	-14.8
03AM148	36 27.88	116 28.58	695.2	979600.04	-43.8	0.0D	0.2	-122.2	-13.8
03AM149	36 27.98	116 28.40	695.1	979600.35	-43.7	0.0D	0.2	-122.1	-13.6
03AM150	36 28.07	116 28.22	694.9	979600.41	-43.8	0.0D	0.2	-122.2	-13.6
03AM151	36 28.16	116 28.03	694.7	979600.17	-44.3	0.0D	0.2	-122.7	-13.9
03AM152	36 28.25	116 27.86	690.7	979600.81	-45.0	0.0D	0.2	-122.9	-14.1

Note: Latitude and longitude of stations in degrees North and degrees West, respectively. Terrain corrections: HAND denotes inner zone correction; TOT is total terrain correction. BOUG ANOM is the complete Bouguer anomaly (reduction density of 2670 kg/m^3); ISOST ANOM is the isostatic residual gravity anomaly.